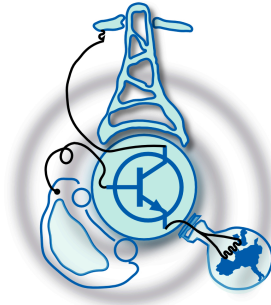


Electromechanical and Thermal Model of Squirrel Cage Induction Machines and Online Parameter Estimation Methods

by
Edson de Souza Lima Junior



Submitted to the Department of Electrical Engineering, Electronics,
Computers and Systems

in partial fulfillment of the requirements for the degree of
Master in Electrical Energy Conversion and Power Systems

at the
UNIVERSIDAD DE OVIEDO

July 20

© Universidad de Oviedo 20. All rights reserved.

Author

Certified by

Juan Manuel Guerrero Muñoz
Associate Professor
Thesis Supervisor

Certified by

Iker Muniategui Aspiazu
Company Coordinator
Thesis Supervisor

Electromechanical and Thermal Model of Squirrel Cage Induction Machines and Online Parameter Estimation Methods

by

Edson de Souza Lima Junior

Submitted to the Department of Electrical Engineering, Electronics, Computers and
Systems
on July 22, 2020, in partial fulfillment of the
requirements for the degree of
Master in Electrical Energy Conversion and Power Systems

Abstract

In this thesis, a multi-domain induction machine model is developed. To get to the final model, the modeling process goes through several steps, with different levels of complexity. First the single-phase equivalent circuit of the induction machine is analyzed, without and with the iron losses equivalent resistor. After, a dynamic model is implemented, also with the option of to consider or not the iron losses. Then, in a different physical domain, a thermal model is implemented through a lumped parameters thermal circuit, that can simulate the temperature in different parts of the motor during the simulation, interacting with the electrical domain through the changes in the values of resistances, depending on the temperature. After all, some online parameter estimation methods were reviewed and one of them were implemented, and validated with simulations.

Thesis Supervisor: Juan Manuel Guerrero Muñoz
Title: Associate Professor

Thesis Supervisor: Iker Muniategui Aspiazu
Title: Company Coordinator

Acknowledgments

First and above all I thank God for my life, health and strength for going through all the professional and personal challenges during this Master's degree.

I thank my supervisor, professor Juan Manuel Guerrero Muñoz for all his wise advice during the development of this thesis and also professor Fernando Briz del Blanco for following the development of the work and making significant contributions. Also special thanks to Ingeteam, represented by the company coordinator Iker Muniategui Aspiazu, for this thesis proposal.

I also would like to thank my parents, Edson and Ana, and my sister Elaine for their unconditional love and support.

I thank my colleagues from the University of Oviedo and the AECP laboratory for their friendship and support.

A special thanks to my dear friend Emanuel Munoz and his beloved family for giving me the emotional, spiritual and personal support to go through my toughest moments.

List of Symbols

B	Damping coefficient of the friction torque [$\frac{N.m}{rad/s}$]
d_b	Average bearing diameter [m]
f_s	Stator frequency [Hz]
i_r	Rotor current [A]
i_s	Stator current [A]
L_r	Rotor's leakage inductance [H]
L_s	Stator's leakage inductance [H]
ℓ	Length [m]
P	Number of poles of the induction machine
P_{gap}	Power transferred through the air gap of the induction motor [W]
P_{iron}	Iron losses in the induction machine [W]
P_{loss}	Total losses of the induction motor [W]
P_{stator}	Joule losses in the stator of the induction machine [W]
R_m	Equivalent resistance for the iron losses [Ω]
R_r	Rotor's single-phase resistance, referred to the stator [Ω]
R_s	Stator's single-phase resistance [Ω]
R_{th}	Thermal resistance [K/W]
r	radius [m]

V_m	Voltage in the magnetizing branch of the induction machine's equivalent circuit [V]
V_s	Stator RMS phase voltage [V]
Z_{eq}	Equivalent phase impedance of the induction machine [Ω]
α_r	Rotor natural frequency [Hz]
r_δ	Average radius of the air gap [m]
δ	air gap
η	Efficiency of the induction motor [%]
θ_f	Average temperature rise of the frame [K]
θ_{i_s}	Angle of the current i_s relatively to the voltage V_s
$\theta_{\varphi_{ri}}$	Phase-shift between the estimated and the reference rotor flux. [rad]
λ	Thermal conductivity [W/m.K]
τ_r	Rotor time constant [s]
φ_r	Rotor flux vector
φ_s	Stator flux vector
φ_{ri}	Rotor flux vector, calculated by the current model of the induction motor
φ_{rv}	Rotor flux vector, calculated by the voltage model of the induction motor
ω	Angular speed [rad/s]
ω_r	Rotor speed [rad/s]
ω_s	Rotor's slip frequency [rad/s]

\Re Real part of a number

Contents

1	Introduction	17
1.1	Literature Review	19
1.2	Research Motivation	22
1.2.1	Research Objectives Before and After Covid-19 Pandemic	22
2	Electromechanical Model of the Induction Machine	25
2.1	Equivalent Circuit	26
2.2	Dynamic Model of the Induction Machine	30
2.2.1	Implementation Without Iron Losses	31
2.2.2	Implementation With Iron Losses	34
2.3	Saturation	37
3	Thermal model of the induction machine	43
3.1	Thermal Network Theory	44
3.2	Induction Machine Thermal Network	46
3.2.1	Machine's geometry and characteristics	48
3.2.2	Thermal resistance between the frame and the ambient (R_{th1})	50
3.2.3	Thermal resistance between the frame and the stator yoke (R_{th2})	51
3.2.4	Thermal resistance between the stator yoke and the stator teeth (R_{th3})	51
3.2.5	Thermal resistance between the stator teeth and the embedded windings (R_{th4})	52

3.2.6	Thermal resistance between the embedded windings and the end windings (R_{th5})	52
3.2.7	Thermal resistance between the rotor and the frame (R_{th6}), rotor and windings (R_{th7}), and between frame and end windings (R_{th8})	53
3.2.8	Thermal resistance between the rotor and the stator teeth (R_{th9})	55
3.2.9	Thermal resistance between the rotor and the bearings (R_{th10})	55
3.2.10	Thermal resistance between the bearings and the frame (R_{th11})	56
3.3	Simulation Results for the thermal circuit	56
4	Online Parameters Estimation	59
4.1	Importance and Main Concepts	59
4.2	Main Parameter Estimation Techniques	61
4.2.1	Spectral Analysis Techniques	61
4.2.2	Observer-based Techniques	62
4.2.3	Model Reference Adaptive System-Based Techniques	63
4.2.4	Other Methods	63
4.3	Model Reference Adaptive System Applied to Parameter Estimation .	64
4.3.1	Estimation's Design	64
4.3.2	Observation of the Rotor Flux	70
4.4	Simulation Results	72
4.4.1	Open Loop Voltage Model as Reference	73
5	Conclusion	75
5.1	Future Work	76
A	Matlab Source Code for Induction Motor Equivalent Circuit Analysis	77
B	Material Properties	81

List of Figures

1-1	Characteristics of the Induction Machine	18
1-2	α -axis simplified IM representation, with $\epsilon = 1$. The β -axis representation is obtained by replacing α components by β components of the same variable and v.v. with $\epsilon = -1$. [11]	20
1-3	α -axis representation with core losses resistor. The β -axis representation is obtained by replacing α components by β components of the same variable and v.v. with $\epsilon = -1$. [11]	21
1-4	Timesheet of the first plan made for the prototype development.	23
2-1	Single-phase equivalent circuit of the induction motor	26
2-2	Representation of the power flow, and the losses in the induction motor.	27
2-3	Mask of the model implemented in Simulink. The model allows the connection of a load, Simulink electrical connections for the stator connections, and also has an output for the most important measurements.	31
2-4	Two tabs of the Simulink's prompt window for the dynamic model implemented.	32
2-5	AC current response for direct start: both Simulink's motor and the implemented model have the same response	33
2-6	Torque response for direct start: both Simulink's motor and the implemented model have the same response	33
2-7	Speed response for direct start: both Simulink's motor and the implemented model have the same response	34

2-8	Current response to direct start. The model with iron losses has a different transient, keeping the higher currents for longer. However, the transient time is nearly the same.	35
2-10	Speed response to direct start. The model with iron losses takes longer to get to the steady-state speed, but has less overshoot, what makes the transient time to be practically the same.	36
2-9	Torque response to direct start. The model with iron losses seems to delay the torque response, but the last part of the transient response is quicker, maintaining practically the same settling time.	36
2-11	Saturation curve obtained from the data of table 2.5.	39
2-12	Values of L_m sampled at 30Hz during the induction motor's direct start, over the saturation curve	40
2-13	Start current for the three models	40
2-14	Start speed for the three models	41
2-15	Start torque for the three models	42
3-1	Thermal network model for induction machines with cage rotor.	47
3-2	Technical drawing of the machine's stator yoke.	49
3-3	Technical drawing of the stator's teeth	50
3-4	Technical drawing of the stator's slot	50
3-5	Y- Δ transformation. It eliminates one node in the thermal circuit.	53
4-1	Effect of detuned parameters in the commands applied by the controller. dq*-axis assumed by the controller in the rotor field oriented control differ from the real position.	60
4-2	Schematic resume of the methods reviewed in this work.	61
4-3	MRAS: The reference model should be independent of α , while the adjustable model depends on it. From the two models, Ψ is obtained and compared. The difference is used to adapt the value of α in the adjustable model.	64
4-4	Rotor flux obtained from the current model	65

4-5	Estimation of the rotor resistance from the phase-shift between the real rotor flux and the estimated rotor flux.	66
4-6	Operation of the closed-loop control in the correction of $\hat{\alpha}_r$	67
4-7	Mismatch in the flux magnitude after the correction of $\hat{\alpha}_r$	67
4-8	Simultaneous estimation of the rotor resistance and the magnetizing inductance	68
4-9	Parallel estimation of R_r and L_m - Measured flux as reference.	72
4-10	Parallel estimation of R_r and L_m - Open loop voltage model as reference.	73

List of Tables

2.1	Machine parameters - single phase equivalent circuit	32
2.2	Nameplate data of the induction machine	32
2.3	Comparison between the values obtained by analysis of the equivalent circuit, and the ones obtained with the steady-state values of the dynamic model implemented in Simulink - Without iron losses	35
2.4	Comparison between the values obtained by analysis of the equivalent circuit, and the ones obtained with the steady-state values of the dynamic model implemented in Simulink - With iron losses	37
2.5	Values of L_m depending on the peak value of the stator current.	38
3.1	Equivalent elements and units between a thermal and an electrical network.	45
3.2	Main characteristics of the motor's geometry	49
3.3	Values of thermal resistances calculated for the modeled motor	57
3.4	The values of temperature for the motor modeled in this work are compared with a different motor of the same rated power, used in the reference paper [12].	57
4.1	Steady-state error with and without online parameter estimation for the simulation of Fig. 4-10.	74
B.1	Material Thermal Data [12]	81

Chapter 1

Introduction

In the field of electrical engineering, one of the widest topics is the simulation and control of induction motors. It's estimated that more than 50% of all the electrical energy produced is consumed by motors [26], and induction motors are one of the most widely used in electrical drives because of their reliability, robustness and relatively low cost. Worldwide the amount of research groups, companies, universities and other institutions that develop some research about the induction motor is really significant. As an example, a quick search on the article basis of IEEE about "Induction Motor" returns almost 33,000 results, among conference papers, journals, books, magazines and others (by 22/07/2020). All this effort applied in research has brought many benefits to the applications where induction machines are used. Even though the induction motors started to be extensively used by the industry in the beginning of the 20th century, their use was very limited, until power electronics started to be applied to control them, almost one century later.

Before the frequency converters, the induction motor use was very limited to some specific applications, for the difficulty to control mainly speed and torque. After these barriers were broken by the frequency converters, a whole new world was open for the application of induction machines. With the time, these machines became also a very good option for the use in traction vehicles, like bicycles, motorcycles, cars, buses, trains and so on.

Thanks to the application of power electronics in the control of the induction

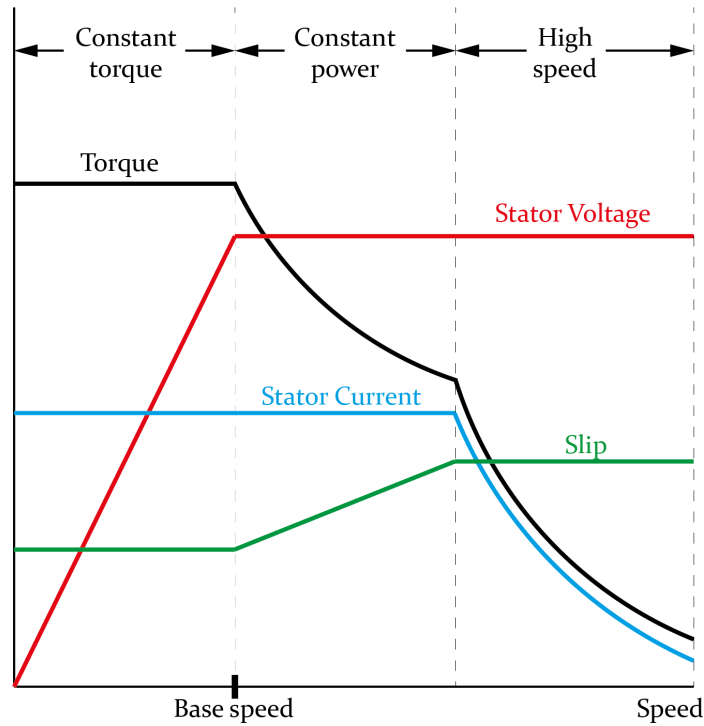


Figure 1-1: Characteristics of the Induction Machine

machine, it can work with the characteristics shown in Fig. 1-1.

As the technology advances and new researches arise, it's more and more important to have simulation models that can represent an induction machine with more fidelity, and showing different aspects of the real machine, in multi-domain simulations, like mechanical, thermal and electrical domains. There are many different simulation softwares in the market, with a large variety of complexity levels. One of the most used softwares, and also the main one used to validate electromechanical control systems in the AECP ("Accionamientos Eléctricos y Convertidores de Potencia") research group, in the University of Oviedo is Matlab Simulink[®]. Because of the need to research about online parameters estimation and temperature estimation in the rotor of induction machines, the asynchronous machine provided by Simulink wouldn't be enough to develop those researches. Unprovided of a thermal model, and also of iron losses, a new model was necessary, and that was where the efforts were put in the development of this work.

1.1 Literature Review

The modeling of induction machines is a very mature field in electrical engineering nowadays. There are many different approaches used to model an induction machine, some of them are only valid for steady-state analysis, as it is the case of the classical single-phase equivalent circuit, presented in Chapter 2 in this Master's Thesis. This kind of circuital approach, however, doesn't consider important variables like magnetic saturation, that can considerably affect the final results. However, the single-phase equivalent circuit is still the fastest methodology that can be adopted to predict the steady-state performances of an induction machine in a wide range of operating conditions [17]. Nevertheless, a dynamic model of the induction motor is still needed in order to simulate its behavior during transients, what allows the execution of realistic simulations, predicting the machine's behavior in real applications, and supporting the research in this field. A reliable electrical drive control system highly depends on its accurate design. The basic engineering design steps to build any system are the schematic diagram, the circuit diagram and the mathematical equations representing that system. So, a good and accurate mathematical model of the motor brings strong consequences to the control implementation, mainly over the control robustness, reliability and the system's overall efficiency.

Regarding dynamic models of induction machines, there are many techniques used to model it and many of them are still being developed, like the use of magnetic reluctance network theory [19]. Regarding the representation of the equations that define a machine, the state-space representation is often used, for its simplicity and low computational effort [1]. The most used approach is the representation of the motor equations in complex vector notation. The development of this theory can be found in many engineering books, like [21] and [9]. This notation comes from the application of axes transformations or reference frame theory, and constitutes an essential aspect of machine analysis. The use of complex vectors provides a very useful and compact form of the machine equations for uniform air gap machines. It's a concept first introduced by Lyon [16]. The complex vector theory provides a

compact notation, easy algebraic manipulation, very simple graphical interpretations and often a very logical and direct development of concepts which are difficult to develop using real variable analysis [21].

In this work, the dynamic model used is an adaptation of the classical dynamic model whose development can be found in many books, like [21] as an example. The classical model doesn't consider iron losses, and its electrical equations are represented by the circuit shown in Fig. 1-2.

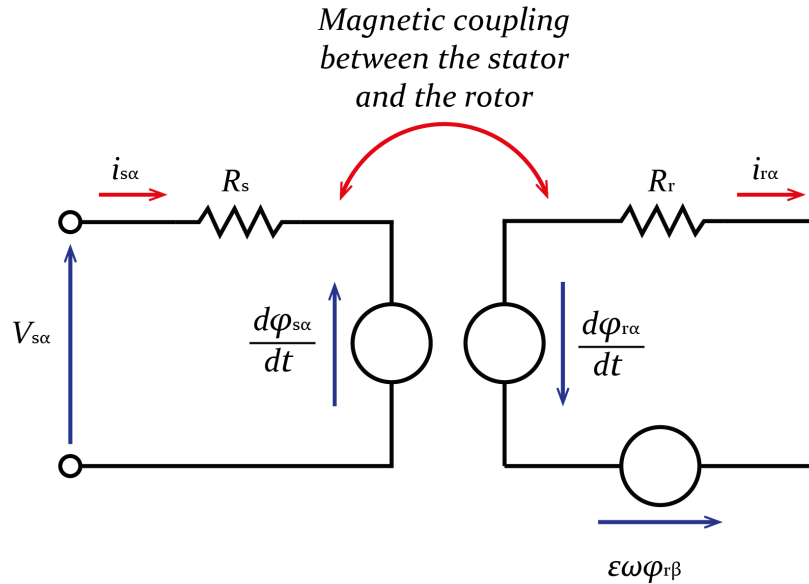


Figure 1-2: α -axis simplified IM representation, with $\epsilon = 1$. The β -axis representation is obtained by replacing α components by β components of the same variable and v.v. with $\epsilon = -1$. [11]

The approach used to introduce iron losses in this model was the direct introduction of the resistance R_m in the model, like in [13]. It's represented as a parallel branch as shown in Fig. 1-3, and very similar to the representation in the induction motor equivalent circuit of Fig. 2-1.

The effect of the resistance R_m in the dynamic model is directly related with the current flowing through the stator inductance, that becomes $i_{2s\alpha}$ instead of $i_{s\alpha}$ (the same way, in β coordinates, $i_{2s\beta}$ instead of $i_{s\beta}$). This is the approach chosen for the development of the model used in this Master's Thesis.

There are other different methods to represent the core losses in the induction

machine, like the method of the equivalent torque, obtained by computing the ratio of the core losses and the motor speed. The resistive torque equivalent to the losses is deducted from the electromagnetic torque in the mechanical equations [11].

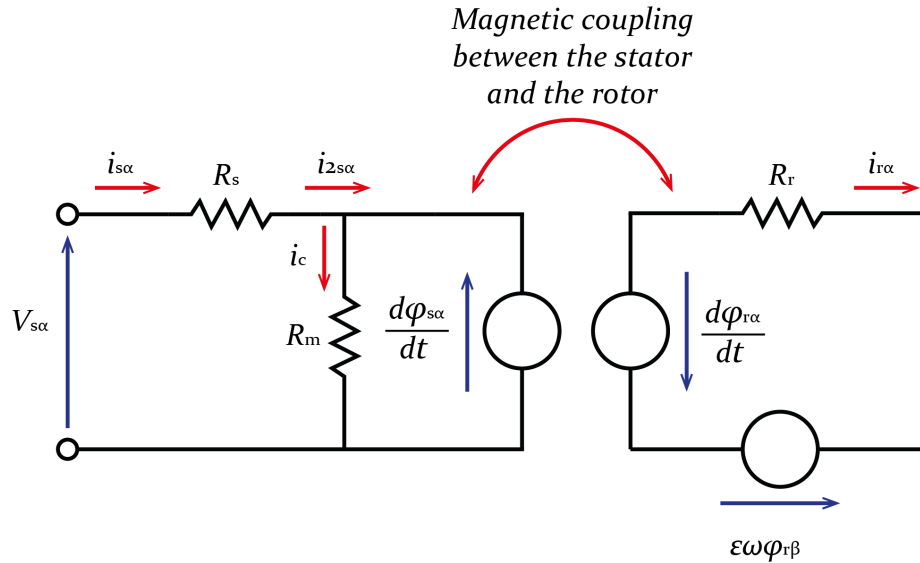


Figure 1-3: α -axis representation with core losses resistor. The β -axis representation is obtained by replacing α components by β components of the same variable and v.v. with $\epsilon = -1$. [11]

Chapter 3 will deal with a different kind of machine modeling, more related with physical properties of the machine materials. It is the thermal model of the induction machine. In this field there are also many different techniques to get to a reliable model, and the variables are even more complex and difficult to measure, like the quality of the materials used in the motor's construction, their volume, physical constitution, etc. The kind of model chosen to be developed in this work was a thermal network of lumped parameters. Many different researchers have developed studies on this topic, like [22] and [3], some of them proposing very sophisticated thermal networks, suitable for several different electric machine types. Some of these models may be very complex, taking into consideration many different aspects of the physical construction of the motor, and having dozens of elements in the equivalent thermal circuit. Also, there are simpler thermal networks that present very good results, like the ones proposed by [3] and [12]. The accuracy of the thermal network, it doesn't matter if it's a sophisticated or a simple one, often depends on several parameters,

for which reliable data may be difficult to find. So the designer's experience plays an important role in the development of the thermal network.

Chapter 4 deals with methods for online parameter estimation in the induction motor. Thanks to the implementation of variable parameters through magnetizing inductance saturation and thermal effect over resistances, these methods can be tested in the proposed model. The own chapter brings a review about methods and literature references, so it will be discussed in that chapter.

1.2 Research Motivation

This Master's Thesis was first proposed with the objective of designing and constructing a traction inverter prototype for railway applications. Traction inverters have several intrinsic characteristics that should be taken into account, and if they are designed for railway applications, there are even more particularities to consider. This has been a hot topic in power electronics field in the last years, due to environmental issues, laws and incentives all around the world related to alternative fuels and advanced vehicles, etc. So, in a competitive market as it is the use of electric drives in railways, every detail counts, in the running towards an efficient, cost-effective and competitive technology.

Nowadays it's impossible to think of efficiency in electrical drives without a proper control design, and without knowing well the characteristics of the motor, the feeding system and the load. That was the idea behind the inverter prototype, to emulate all these components and research improvements that at the end would lead to one main goal: efficiency.

1.2.1 Research Objectives Before and After Covid-19 Pandemic

In the month of February of 2020, the first planning was made to the development of the prototype. The timesheet of Fig. 1-4 shows the plan made at the time.

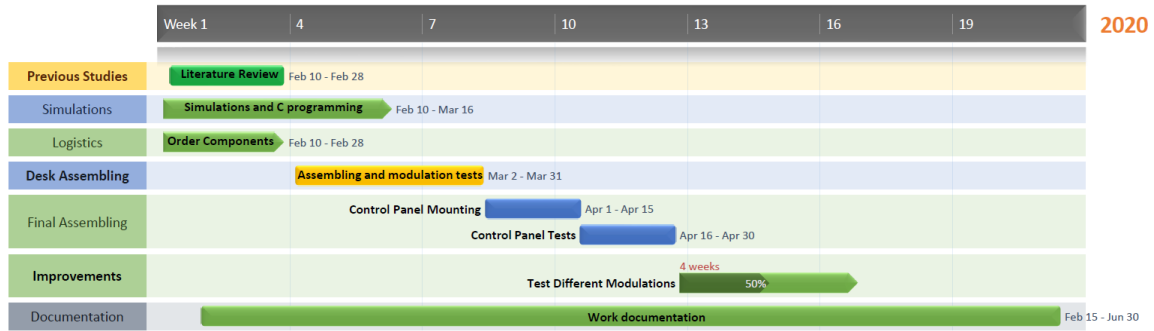


Figure 1-4: Timesheet of the first plan made for the prototype development.

At the end of the month of February, with the spread of Covid-19 pandemic, the first contingencies started to appear, by the delay in the delivery of components ordered. Then, in March 14, the government of Spain decreed state of alarm in all the country, closing all the public institutions, including the University Oviedo, and all its laboratories. Facing the uncertainty of when the situation, the scope of the Master's Thesis was changed to a related topic, but without the physical implementation part, being based only on computational simulations. So, instead of the simulated control of an induction machine, the focus was changed to the development of a simulation model of the induction machine, with more possibilities than the model offered by Matlab Simulink[®]. First, model with iron losses was implemented, then a thermal model, and after, to make use of these models, the parameter estimation method was implemented.

Chapter 2

Electromechanical Model of the Induction Machine

The design of an electromechanical model of the induction machine was motivated in this work by the absence of a complete model in the simulation software used in this work, MATLAB Simulink. For the proposed work, the induction motor simulation model should have the following features:

- Variable stator and rotor resistances, changing depending on the stator/rotor temperature;
- A thermal model of the induction machine, to make the resistances change over a realistic curve;
- Iron losses, because these are important in the thermal model, and how the temperature changes in each part of the motor.
- Saturation of the magnetic material, so the mutual inductance L_m changes depending on the flux, also approximating the behavior of the real motor.

In Simulink, up to the date this work was started (March of 2020), among these characteristics, only the core saturation was available. So it was convenient, even for future works, to build a brand new model in Simulink's environment including all of these features. The next sections in this chapter show how this model was developed. And a full chapter (Chapter 3) was dedicated to the thermal model of the induction machine.

2.1 Equivalent Circuit

The induction machine's model developed in this work begins by the per-phase equivalent circuit model [7]. It is the simplest way to model an induction machine. The circuit is shown in Fig. 2-1. From this circuit, many characteristics of the induction machine can be obtained, like stator's current, rotor's current, Joule losses, iron losses, torque and speed. The inputs for the circuit are the steady-state values of the the fundamental voltage component, and the rotor speed.

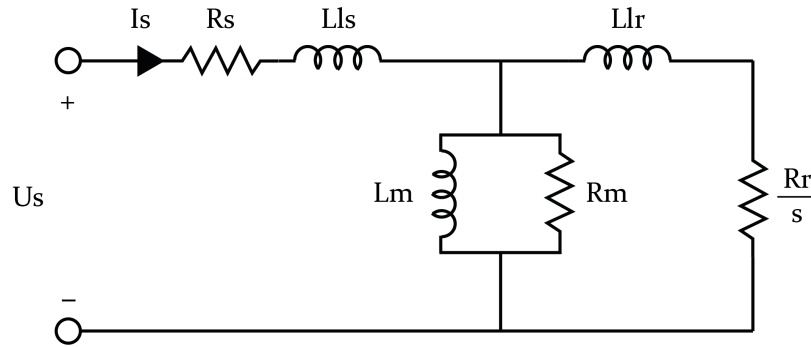


Figure 2-1: Single-phase equivalent circuit of the induction motor

The machine's parameters needed to build this model are the stator resistance (R_s), the stator leakage inductance (L_{ls}), the magnetizing inductance (L_m), the equivalent iron losses resistance (R_m), the rotor leakage inductance (L_{lr}) and the rotor resistance (R_r). Considering these parameters, a simple circuit analysis can give all the steady-state values for any machine, if the parameters are well represented.

In order to check the model implemented in Simulink, a Matlab script was made to run the steady-state circuit analysis for given parameters. The script can be verified in Appendix A. The equations that based the script are detailed below in this section.

Electrical Steady-State Values

From the equivalent circuit, the rated phase current of the induction machine will be

$$i_s = \frac{V_s}{Z_{eq}} \quad (2.1)$$

where V_s is the RMS value of the phase voltage in the stator, and Z_{eq} is the equivalent phase impedance, given by

$$Z_{eq} = (R_s + j2\pi f_s L_{ls}) + \frac{\left[\frac{R_m \cdot j(2\pi f_s L_m)}{R_m + j(2\pi f_s L_m)} \right] \cdot \left[\frac{R_r}{s} + j(2\pi f_s L_{lr}) \right]}{\left[\frac{R_m \cdot j(2\pi f_s L_m)}{R_m + j(2\pi f_s L_m)} \right] + \left[\frac{R_r}{s} + j(2\pi f_s L_{lr}) \right]} \quad (2.2)$$

The rated active power P_{in} and reactive power S_{in} are given by equations 2.3 and 2.4 respectively.

$$P_{in} = |3V_s i_s| \cos(\theta_{i_s}) \quad (2.3)$$

where θ_{i_s} is the angle of the stator current i_s relatively to the voltage V_s .

$$S_{in} = |3V_s i_s| \quad (2.4)$$

Losses in Steady-State

For the equivalent model it's also possible to calculate the losses in the induction machine, in steady-state. There are three different kinds of losses that happen due to the electrical parameters. The Joule losses in the stator and in the rotor, and the iron losses, represented by the resistance R_m . Regarding the mechanical losses, in this model, we will consider only the losses due to friction. A more detailed model can be built considering also stray losses. The remaining power is the one transferred mechanically through the shaft of the machine.

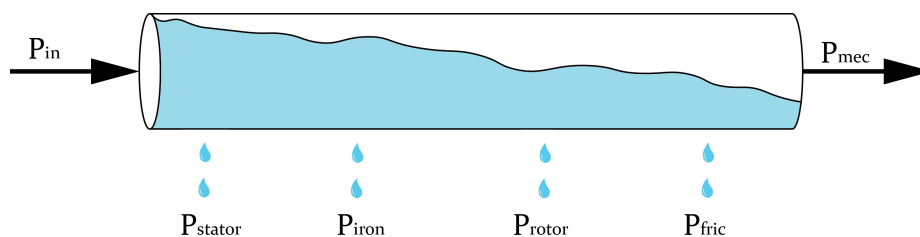


Figure 2-2: Representation of the power flow, and the losses in the induction motor.

This concept can be better understood by the analogy presented in Fig. 2-2. The amount of water that goes in the tube is the total input power. Some of the water

(power) is leaked by Joule losses in the stator, iron losses, Joule losses in the rotor and friction. The water that goes out on the other side of the tube is the mechanical power available in the shaft.

Once the input phase current is the one going through R_s , the Joule losses in the stator (P_{stator}) are straightforward.

$$P_{stator} = \Re(3R_s i_s^2) \quad (2.5)$$

where \Re denotes the real part of the number.

To find the losses in the the rotor, first we define the voltage in the magnetizing branch, that is:

$$V_m = V_s - i_s(R_s + 2\pi f_s L_{ls}) \quad (2.6)$$

And so the current in the rotor will be

$$i_r = \frac{V_m}{\left[\frac{R_r}{s} + j(2\pi f_s L_{lr})\right]} \quad (2.7)$$

With these values, it's possible to find the Joule losses in the rotor, defined by Eq. 2.8.

$$P_{rotor} = \Re(3R_r i_r^2) \quad (2.8)$$

And finally the iron losses can be found by the expression contained in Eq. 2.9

$$P_{iron} = \Re \left[3 \frac{V_m^2}{R_m} \right] \quad (2.9)$$

The last losses considered in this model are the mechanical losses due to friction. These are proportional to the rotor's speed (neglecting the constant term of friction), and can be calculated by [8]:

$$P_{fric} = B\omega_r^2 \quad (2.10)$$

Mechanical Steady-State Values

Regarding the mechanical steady-state values of the induction machine, the parameters needed for the calculations are:

- The rated input voltage frequency (f_s);
- The number of poles of the machine (P);
- The rated rotor's slip (ω_s).

Having these values, the rotor's rated speed is given by Eq. 2.11.

$$\omega_r = \frac{120f_s}{P} \quad (2.11)$$

The rotor slip is commonly given by the manufacturers as a percentage of the rated speed. This is the variable used in the equivalent circuit in Fig. 2-1 and in the steady-state equations, denoted by s .

The mechanical power developed by the motor depends on the total power in the airgap, that is:

$$P_{gap} = \Re \left(\frac{3R_r i_r^2}{s} \right) \quad (2.12)$$

So the mechanical power available in the shaft is finally given by

$$P_{mec} = P_{gap} - P_{rotor} - P_{fric} \quad (2.13)$$

Another important mechanical characteristic of the machine that can be obtained from the equivalent circuit is the developed torque. It is related to the mechanical power P_{mec} and to the rotor speed, and is given by

$$Torque = \frac{P_{mec}}{\omega_r} \quad (2.14)$$

After all these calculations, the overall efficiency of the machine can be evaluated

by the ration between the output power P_{mec} and the input power P_{in}

$$\eta = \frac{P_{mec}}{P_{in}} \cdot 100 \quad (2.15)$$

2.2 Dynamic Model of the Induction Machine

After considering the steady-state analysis of the induction machine, using the equivalent circuit, the next step in the development of the model will be a dynamic model, from which we can obtain also the transient behavior of the machine, apart from the steady-state behavior. This dynamic model is characterized by a set of equations for voltage, current and flux in the stator and in the rotor. By applying direct-quadrature-zero transformation, also called Park transform, we can express those equations in an arbitrary reference frame rotating at the angular speed ω . These equations (Eq.2.16 to 2.23) already consider the iron losses, provided by the resistance R_m in the equivalent circuit of figure 2-1 [11].

Stator and Rotor Flux Equations

$$\varphi_{ds} = L_s i_{ds} - \frac{L_s}{R_m} \left[\frac{d\varphi_{ds}}{dt} - \omega_d \varphi_{qs} \right] + L_m i_{dr} \quad (2.16)$$

$$\varphi_{qs} = L_s i_{qs} - \frac{L_s}{R_m} \left[\frac{d\varphi_{qs}}{dt} + \omega_d \varphi_{ds} \right] + L_m i_{qr} \quad (2.17)$$

$$\varphi_{dr} = L_r i_{dr} + L_m i_{ds} - \frac{L_m}{R_m} \left[\frac{d\varphi_{ds}}{dt} - \omega_d \varphi_{qs} \right] \quad (2.18)$$

$$\varphi_{qr} = L_r i_{qr} + L_m i_{qs} - \frac{L_m}{R_m} \left[\frac{d\varphi_{qs}}{dt} + \omega_d \varphi_{ds} \right] \quad (2.19)$$

Sator and Rotor Electrical Equations

$$v_{ds} = R_s i_{ds} + \frac{d\varphi_{ds}}{dt} - \omega_d \varphi_{qs} \quad (2.20)$$

$$v_{qs} = R_s i_{qs} + \frac{d\varphi_{qs}}{dt} + \omega_d \varphi_{ds} \quad (2.21)$$

$$0 = R_r i_{dr} + \frac{d\varphi_{dr}}{dt} - (\omega_d - \omega) \varphi_{qr} \quad (2.22)$$

$$0 = R_r i_{qr} + \frac{d\varphi_{qr}}{dt} + (\omega_d - \omega) \varphi_{dr} \quad (2.23)$$

2.2.1 Implementation Without Iron Losses

The dynamic equations in dq0 arbitrary reference frame were implemented in Matlab Simulink, using block diagrams. A block was created as shown in Fig. 2-3.

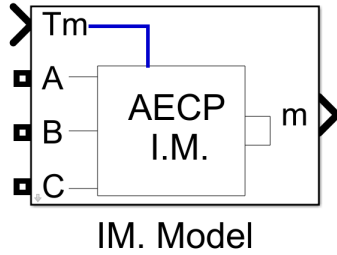


Figure 2-3: Mask of the model implemented in Simulink. The model allows the connection of a load, Simulink electrical connections for the stator connections, and also has an output for the most important measurements.

The model also has a prompt window where it's possible to configure the machine's parameters, shown in Fig. 2-4.

The implementation was made with the option of neglect the iron losses, so it can be compared with the native Simulink's induction machine, that don't have iron losses implemented. The elements of the equivalent circuit were calculated by Tommaso Moretto in [20], and are given as data for the model's calculation. They are as shown in table 2.1.

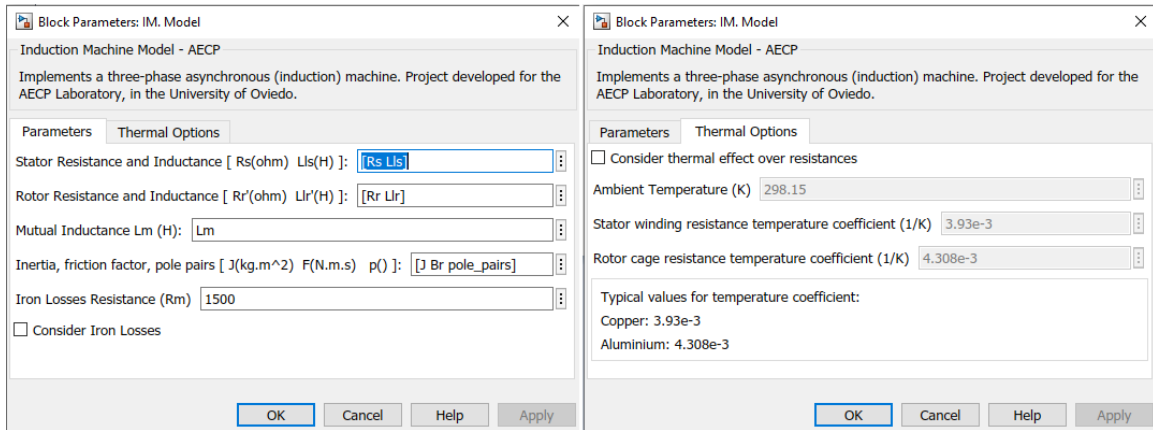


Figure 2-4: Two tabs of the Simulink’s prompt window for the dynamic model implemented.

R_s	R_r	R_m	L_m	L_{ls}	L_{lr}
1.1 [Ω]	0.62 [Ω]	1,500 [Ω]	121.8 [mH]	7.7 [mH]	7.7 [mH]

Table 2.1: Machine parameters - single phase equivalent circuit

This machine is a 4kW induction motor, running in the facilities of the AECP (“Accionamientos Eléctricos y Convertidores de Potencia”) laboratory, in the University of Oviedo. The nameplate data of this machine is in Table 2.2.

V	Connection	Hz	rpm	kW	A	$\cos(\phi)$
230	D	50	1450	4.00	15.20	0.75
400	Y	50	1445	4.00	8.8	0.75
415	Y	50	1445	4.00	9	0.71

Table 2.2: Nameplate data of the induction machine

The simulation for the direct start of the machine, connected to a $400V_{RMS}$ grid is shown in Fig. 2-5.

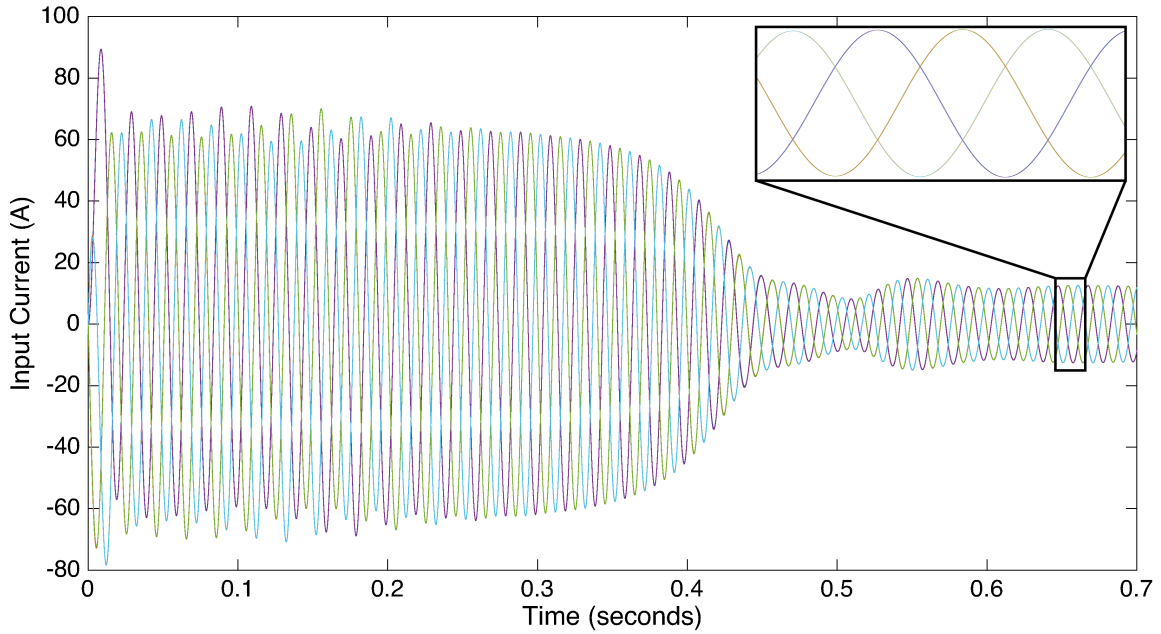


Figure 2-5: AC current response for direct start: both Simulink's motor and the implemented model have the same response

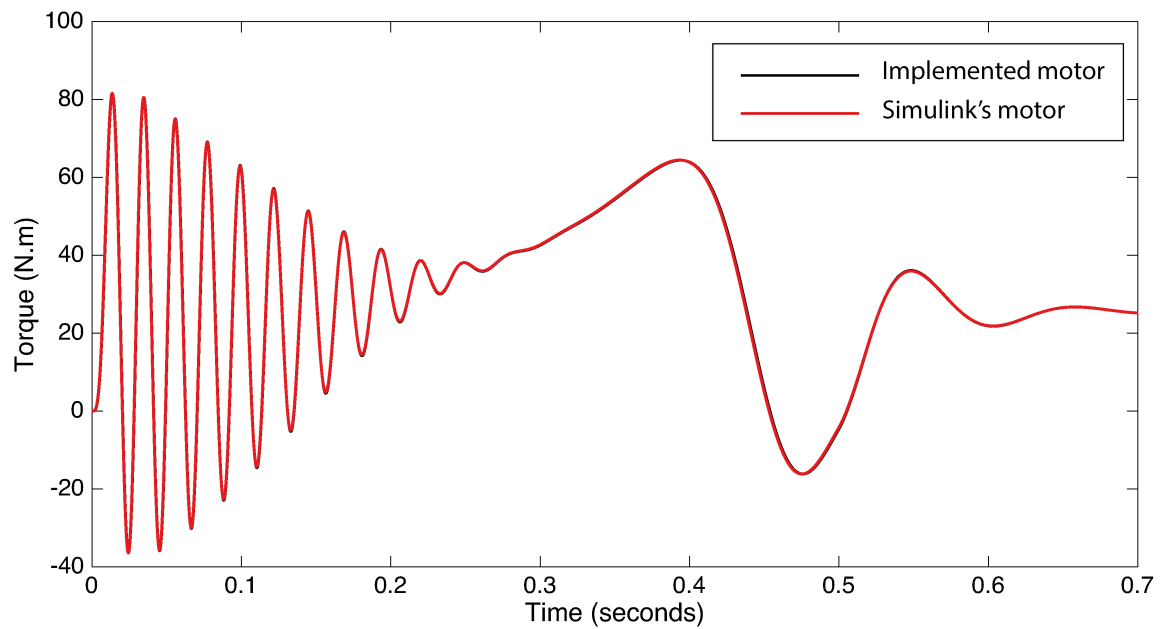


Figure 2-6: Torque response for direct start: both Simulink's motor and the implemented model have the same response

According with this simulation, the machine gets to steady-state in approximately 0.7s. Also, in the zoom shown in the figure, it's possible to see that the currents of

Simulink's induction motor, and the dynamic model implemented are superposed. It means that the implementation made, not considering iron losses, is the same made by the native block of Simulink. The same observation can be made for the torque and speed, respectively in Figs. 2-6 and 2-7.

So by comparing and checking that the motors have the same input current, same torque and same speed, it's also confirmed that they have the same losses, because the input and output power is the same.

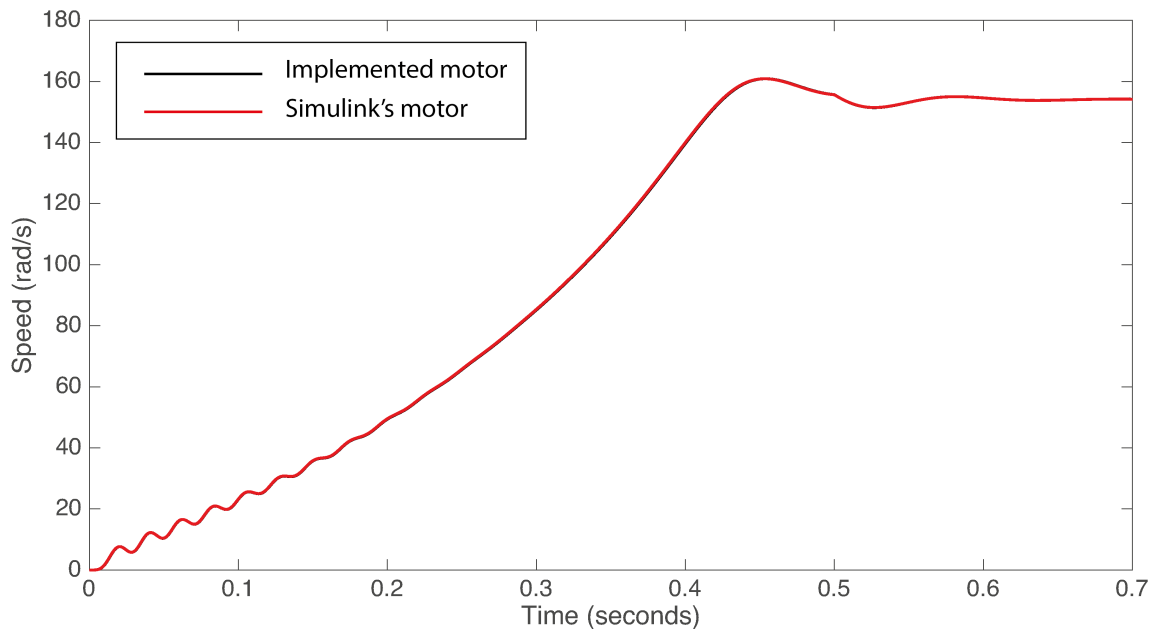


Figure 2-7: Speed response for direct start: both Simulink's motor and the implemented model have the same response

The steady-state values obtained can be compared to the ones obtained by the analysis of the equivalent circuit. The values are presented in Table 2.3.

2.2.2 Implementation With Iron Losses

The next step in the implementation would be to consider the value of the iron losses resistance R_m in the dynamic equations. For the model implemented in Simulink, this option can be activated by checking the check-box of the prompt in Fig. 2-4. In the equivalent circuit, the value of R_m is set to $1,500\Omega$. For this case, the same

	Equivalent Circuit Analysis	Dynamic Model
Torque (N.m)	26.7	26.7
Speed (rpm)	1468.5	1470.6
Input Current (Arms)	8.8	8.98
Power Factor	0.71	0.71
Input Voltage (V)	400	400
Input Power (W)	4,348	4,452
Output Power (W)	4,015	4112
Efficiency (%)	92.3	92.4

Table 2.3: Comparison between the values obtained by analysis of the equivalent circuit, and the ones obtained with the steady-state values of the dynamic model implemented in Simulink - Without iron losses

graphics shown before, comparing Simulink's native motor and the implemented one can be analyzed again.

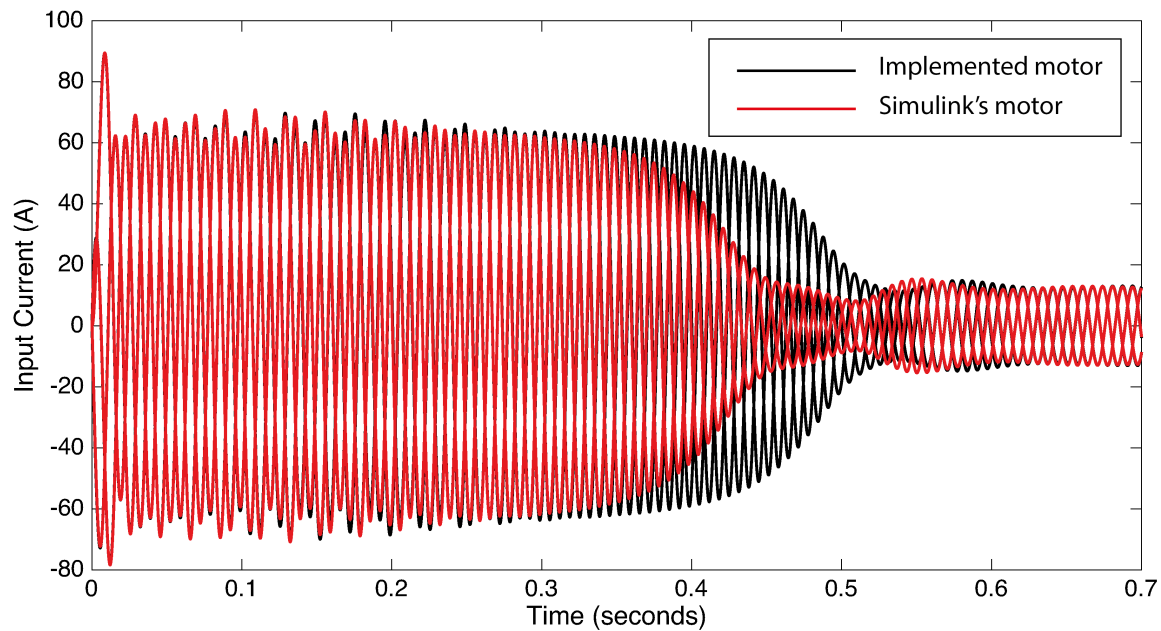


Figure 2-8: Current response to direct start. The model with iron losses has a different transient, keeping the higher currents for longer. However, the transient time is nearly the same.

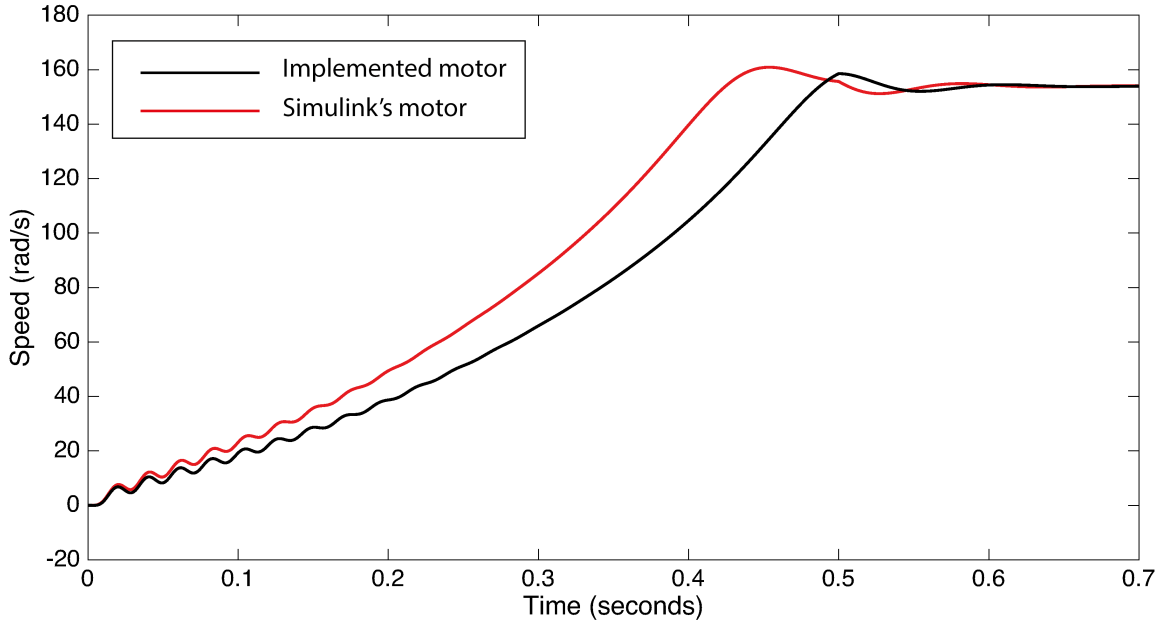


Figure 2-10: Speed response to direct start. The model with iron losses takes longer to get to the steady-state speed, but has less overshoot, what makes the transient time to be practically the same.

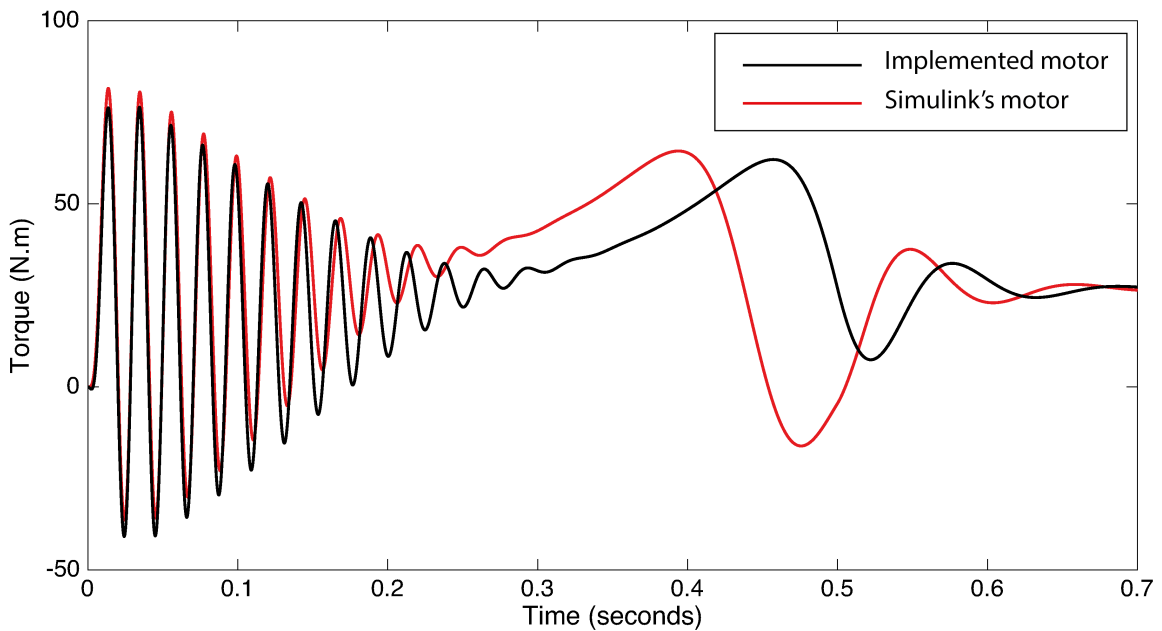


Figure 2-9: Torque response to direct start. The model with iron losses seems to delay the torque response, but the last part of the transient response is quicker, maintaining practically the same settling time.

Also for this case, with iron losses, the steady-state values can be evaluated by

the analysis of the equivalent circuit of Fig. 2-1. In the previous analysis without iron losses, the resistance R_m had its value set to $1 \cdot 10^{10}$, so the losses on in would be negligible. Now, R_m is set to the value found in Table 2.1. The comparison between the equivalent circuit analysis and the results obtained from the simulation of the dynamic model are shown in Table 2.4.

	Equivalent Circuit	Dynamic
	Analysis	Model
Torque (N.m)	26.6	26.5
Speed (rpm)	1468.5	1459.7
Input Current (Arms)	8.91	9.07
Power Factor	0.72	0.73
Input Voltage (V)	400	400
Input Power (W)	4,434	4,432
Output Power (W)	3,998	4086
Efficiency (%)	90.2	92.2

Table 2.4: Comparison between the values obtained by analysis of the equivalent circuit, and the ones obtained with the steady-state values of the dynamic model implemented in Simulink - With iron losses

The results shown for the dynamic model are coherent with the expected ones by the equivalent circuit, and so this implementation is assumed to be correct. The next step in the model of this motor was to implement the saturation of the magnetic material, that would have direct impact on the value of the inductance L_m , and will be discussed in the next session.

2.3 Saturation

Incorporating the saturation of the main flux path is a very common practice in the modeling of induction machines for simulations of steady-state and dynamic behavior. Also, for control purposes like rotor flux oriented control of induction machines, the

saturation is very useful in the model of the machine, because it makes the behavior of the simulated machine to get closer to the behavior of a real machine, that is subject to saturation, depending on the current it drains.

The saturation of the magnetizing inductance, and how to represent it is a topic considered in detail by many authors, and there are many different methods, with different levels of complexity. In the model implemented in this work, it was directly related to the stator current, applying a given magnetizing curve, according with Table 2.5.

Current (A)	L_m (H)
6.47	0.13048064
8.30	0.12863027
11.63	0.12368251
15.53	0.1208373
19.00	0.11755072
22.93	0.11116174
30.77	0.0943646
38.63	0.08111757
48.30	0.06886478
60.63	0.05771421
74.17	0.04909763
90.33	0.0415446
104.00	0.03682519
121.10	0.03215526
135.87	0.0288778

Table 2.5: Values of L_m depending on the peak value of the stator current.

The data of this table yields to the saturation curve of this machine, shown in Fig. 2-11.

So, from this data it is possible to add to the model a Look-up table with the

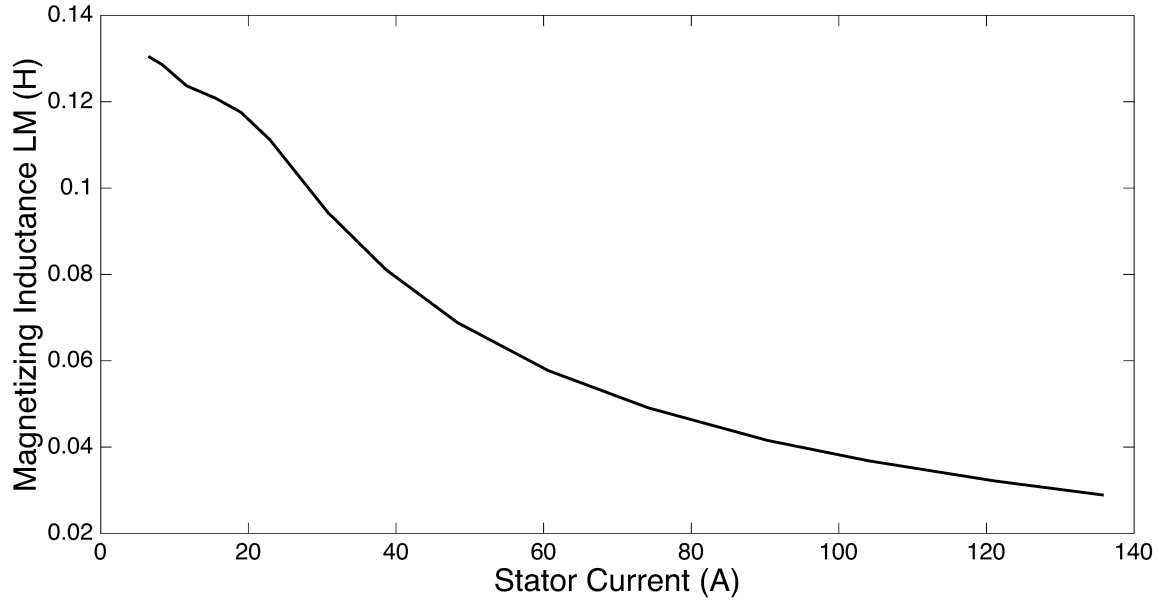


Figure 2-11: Saturation curve obtained from the data of table 2.5.

values of Table 2.5, and the value of L_m for the purpose of the simulation begins to depend on the stator current. The results of this interaction between current and the magnetizing inductance give place to a dynamic behavior of the value of L_m . During the direct start of the machine, the value of L_m changes depending on the current. To understand how this change happens, the values of L_m and i_s were sampled at a frequency of 30Hz, and plotted in Fig. 2-12, together with the magnetizing curve.

As Fig. 2-12 shows, in the direct start of the induction machine, when the current assumes very high levels, the value of L_m is significantly reduced. After this transient time, with the reduction of the rotor slip ω_s , the current reduces to its rated value, and so L_m reaches its steady-state value, close to the rated one.

To analyze the results of having saturation in the induction machine, it's also convenient to perform the same tests made before in the case of iron losses. Now, the three models will be put together in the same graphs:

- Simpler model, without iron losses and without saturation;
- The implemented model with iron losses but without saturation;
- The implemented model with iron losses and saturation.

Results are shown for input current (Fig. 2-13), speed (Fig. 2-14) and torque

(Fig. 2-15).

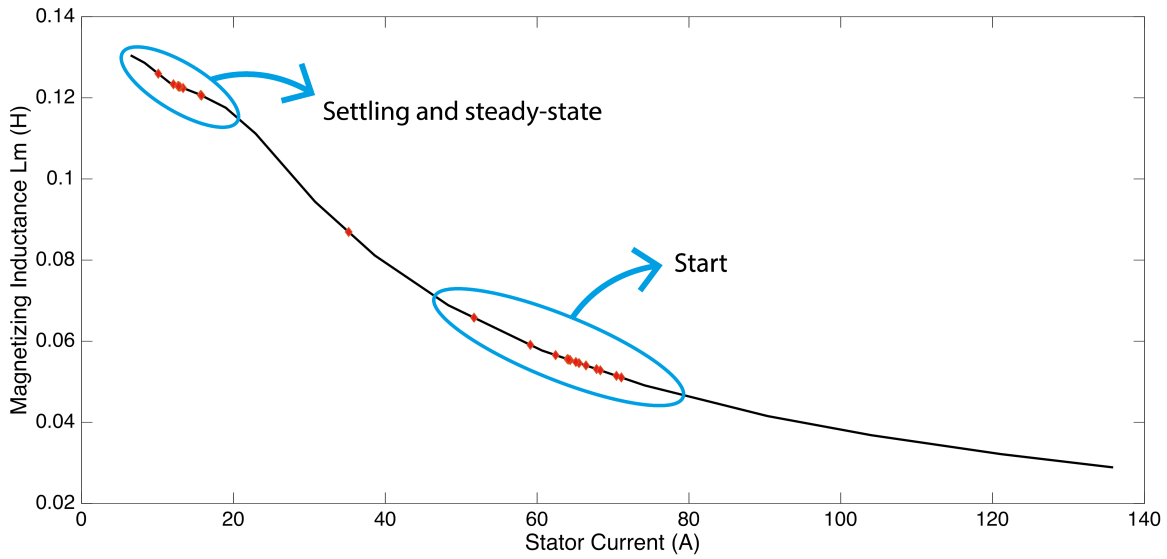


Figure 2-12: Values of L_m sampled at 30Hz during the induction motor's direct start, over the saturation curve

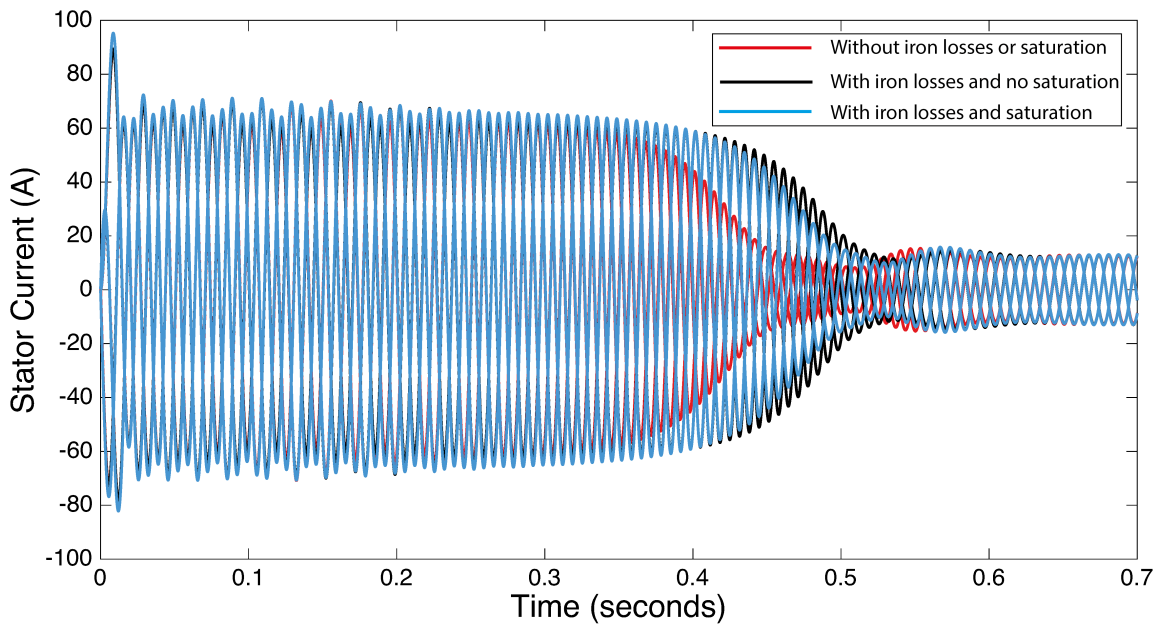


Figure 2-13: Start current for the three models

Knowing that a more detailed model leads to a more realistic simulation, it's possible then to explore more features of the simulations of induction machines. In the next chapters, two different features will be seen in detail. First the thermal

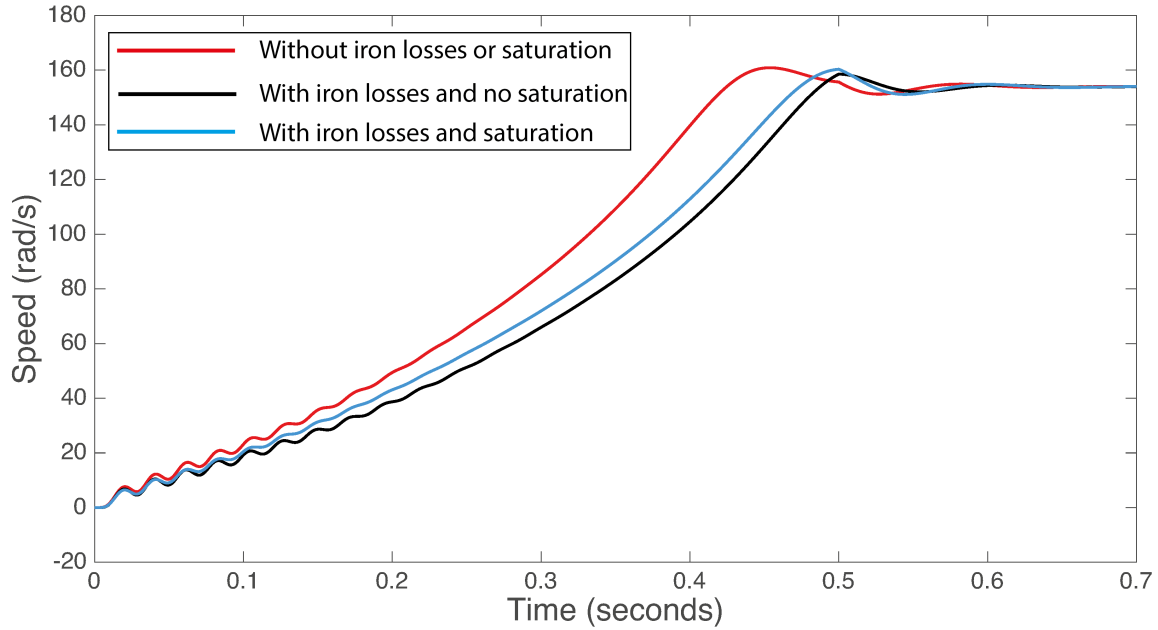


Figure 2-14: Start speed for the three models

model of the induction machine, that has its effect directly related to the values of the resistances in the stator and rotor. And then, in the following chapter, the real-time machine parameter estimations will be discussed. This model, provides more accurate data for the thermal model, once it provides iron losses (that in the end become heat), and also the variation of L_m , useful to test the algorithms of parameter estimation.

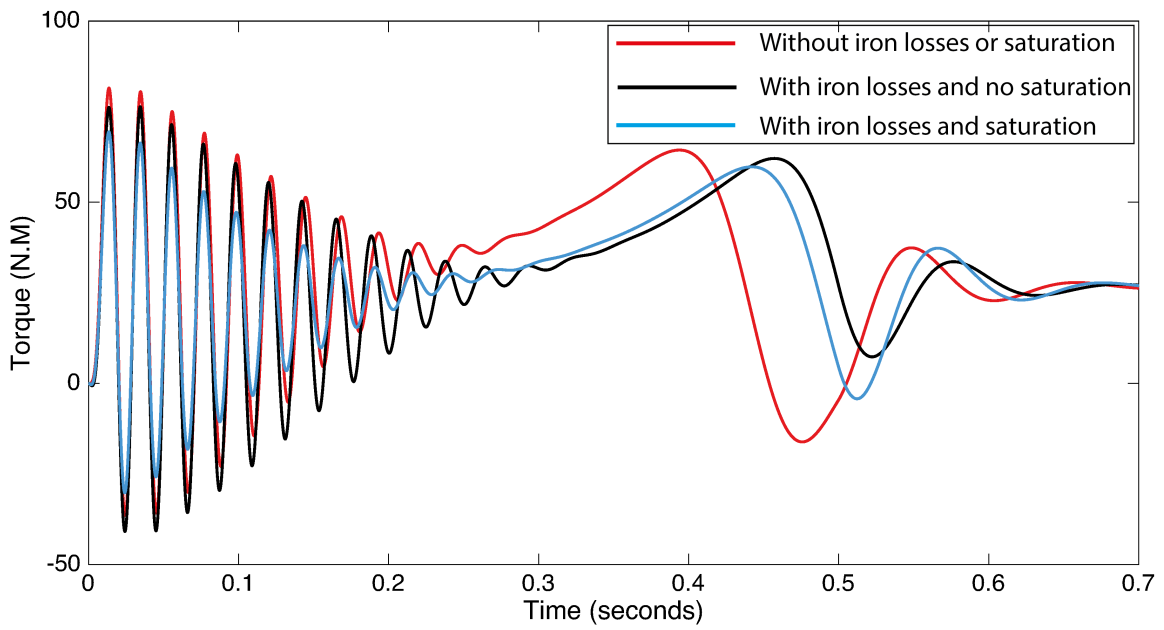


Figure 2-15: Start torque for the three models

Chapter 3

Thermal model of the induction machine

In this chapter, the thermal model of the induction machine will be discussed. The machine considered for this work is a TEFC (totally enclosed fan cooled) machine. This characteristic plays an important role in the thermal model once the air doesn't flow freely through the inside of the machine. Also in this chapter, it is possible to go through the calculation of each of the thermal resistances involved in the thermal circuit.

The considered losses, in this case the sources of heat for the thermal circuit, are the resistive losses in the rotor and in the stator, and the iron losses, represented by the resistance R_m , according with the equivalent single-phase circuit of the induction machine shown in the Fig. 2-1.

The modeled machine is the same 4 kW asynchronous motor, running in the facilities of the AECF research group. The nameplate data of that machine is as shown in Table 2.2. According with these data, the rated torque for this machine is 26.4 N.m.

3.1 Thermal Network Theory

In a thermal network, the whole system is divided into basic thermal elements. These elements form a network composed by thermal resistances and nodes. The nodes represent the different parts of the system, and the resistances represent the opposition to the heat transfer between two nodes. The thermal network can be compared to the electrical network using the analogy presented by Table 3.1. These elements can be compared to electrical components

For induction motors, usually, the air temperature is taken as reference, and a temperature source is added representing the air temperature. The machine elements are then represented by the temperature difference between them and the ambient.

Considering these information, as well as an electrical network, a thermal network can be solved analytically. Let us consider that a thermal network has n nodes, linked to each other by resistances $R_{i,j}$, where i and j are the indexes of the two nodes linked. Also, let us consider that $R_{i,i}$ is the thermal resistance between a node and the ambient. In that case, the steady-state temperature of each node (relatively to the ambient temperature) will be related by [12]:

$$P_i = \frac{\theta_i}{R_{i,i}} + \sum_{j=1}^n \frac{\theta_i - \theta_j}{R_{i,j}} \quad i = 1, \dots, n \quad (3.1)$$

where θ_i is the temperature difference with respect to the ambient in a node, and P_i are the total power losses in a node. With this concept well defined, a conductance matrix can be defined.

$$\begin{bmatrix} \sum_{i=1}^n \frac{1}{R_{1,i}} & \frac{-1}{R_{1,2}} & \frac{-1}{R_{1,3}} & \dots & \frac{-1}{R_{1,n}} \\ \frac{-1}{R_{2,1}} & \sum_{i=1}^n \frac{1}{R_{2,i}} & \frac{-1}{R_{2,3}} & \dots & \frac{-1}{R_{2,n}} \\ \frac{-1}{R_{3,1}} & \frac{-1}{R_{3,2}} & \sum_{i=1}^n \frac{1}{R_{3,i}} & \dots & \frac{-1}{R_{3,n}} \\ \frac{-1}{R_{n,1}} & \frac{-1}{R_{n,2}} & \frac{-1}{R_{n,3}} & \dots & \sum_{i=1}^n \frac{1}{R_{n,i}} \end{bmatrix} \quad (3.2)$$



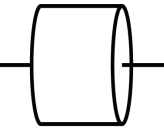
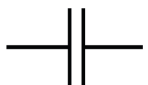
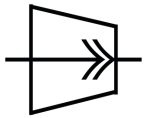
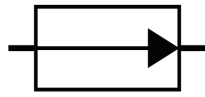


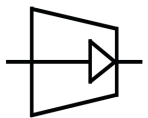
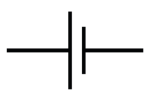
Thermal Network	Electrical Network
 Thermal Resistance	 Electrical Resistance
 Thermal Mass	 Capacitor
 Heat Flow Source	 Current Source
 Absolute Zero	 Ground
 Temperature Source	 Voltage Source
UNIT ANALOGY	
Temperature (K)	Voltage (V)
Heat Flow (J/s)	Current (A)
Therm. Resistance (K/W)	Electrical Resistance (Ω)

Table 3.1: Equivalent elements and units between a thermal and an electrical network.

This conductance matrix makes possible to express the system of equations in a matrix form. In order to do that, we define two column vectors for the losses in each node (P), and the temperature difference of each node with respect to the ambient (Θ).

$$P = \begin{bmatrix} P_1 \\ P_2 \\ P_3 \\ \dots \\ P_n \end{bmatrix} \quad (3.3)$$

$$\Theta = \begin{bmatrix} \theta_1 \\ \theta_2 \\ \theta_3 \\ \dots \\ \theta_n \end{bmatrix} \quad (3.4)$$

So, using these matrices, we can redefine equation 3.1 as

$$P = G\Theta \quad (3.5)$$

$$\Theta = G^{-1}P \quad (3.6)$$

So the stationary solution for the temperatures are obtained directly from Eq. 3.6. Nonetheless it's important to observe that some of the resistances in G , and mainly some of the losses in P are temperature dependent. In this case, for a more complete solution, this parameters should be calculated iteratively, updating the values in these matrices until the error is sufficiently small.

3.2 Induction Machine Thermal Network

The model presented in Fig.3-1 [12] is a thermal network designed to simulate the temperature effect in an induction motor in a simple way, without complex thermal networks. This model neglects the variation of the heat transfer coefficient along the frame. It means that in the axial direction, the machine temperatures will be considered as symmetrical, and each element of the machine will be considered as a whole.

To this model, the asymmetries related to temperature distribution were adjusted by empirical correction factors. Similar models were proposed by Champenois et al. [4] and Mellor et al. [22].

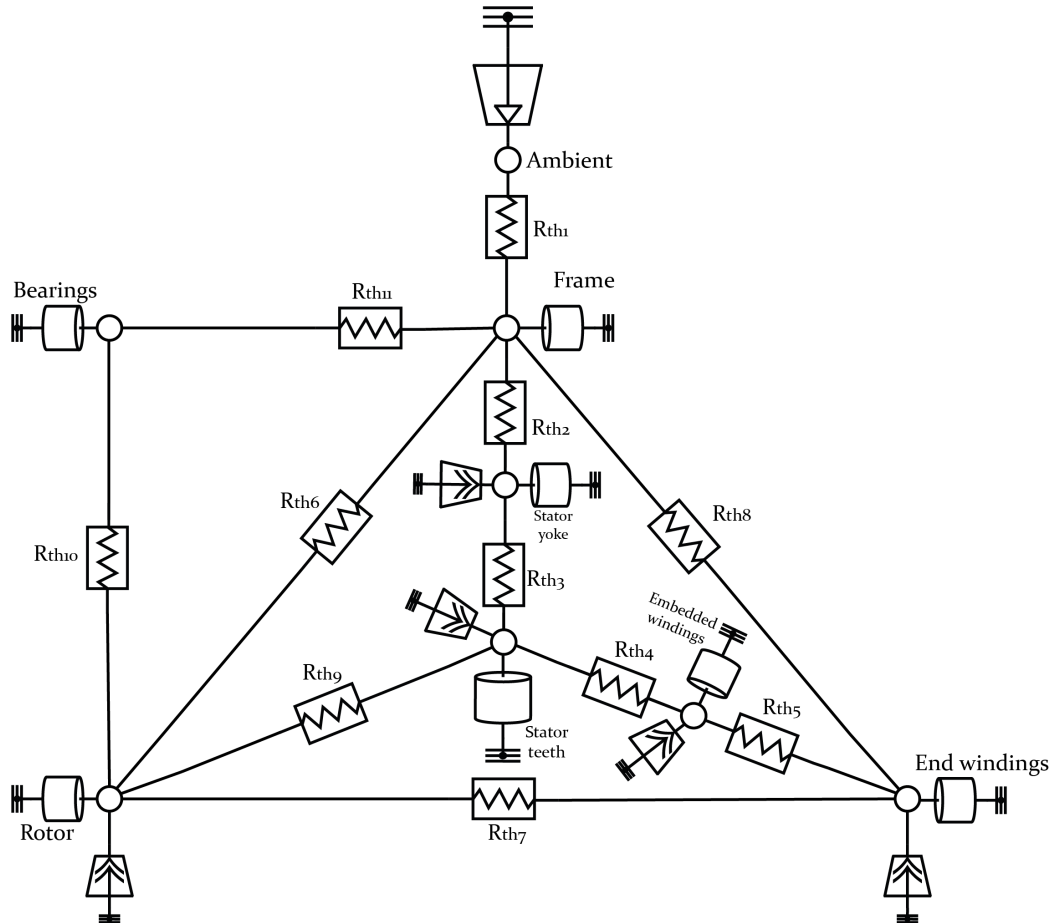


Figure 3-1: Thermal network model for induction machines with cage rotor.

It is valid to say that when it comes to lumped parameters thermal models, the designer's experience plays a great role in the accuracy of the model both in analytical and numerical approaches [3]. This happens because of the asymmetries present in every machine due to the manufacturing process, like the smoothness of the outer stator lamination and the inner housing surface. Despite of the use of more sophisticated approaches to model the induction machine thermal circuit, like more complex thermal networks, or finite elements, if the thermal circuit has a good design, its accuracy has been already tested for machines as big as 1 MW [3].

In this model, the rotor is lumped into one unique element, not making any differ-

ence between the cage and the rotor core. The rotor temperature then corresponds to the average temperature in the rotor surface. The internal air is not represented in the circuit, however it is considered in the previous calculations. After those calculations, a Y- Δ transformation is made and eliminates the internal air node.

The model has one temperature source in the ambient, that will be the reference for all other elements. Also there are 5 heat flow sources, that represent the losses in different parts of the motor: copper losses in the end and embedded windings, aluminum losses in the rotor, and iron losses in the stator yoke and stator teeth.

It's recommended [12] to determine R_{th1} and R_{th4} from measurements, and then use the manufacturer's data, or measurements to calculate all other thermal resistances, once they depend exclusively on the machine's geometry and material.

In the following subsections of this chapter, the process of calculation of each of the thermal resistances in the circuit will be described.

3.2.1 Machine's geometry and characteristics

In this sections, the main dimensions of the considered machine will be presented. Later in this chapter, these dimensions will be used to characterize the thermal resistances of the circuit. To calculate the thermal circuit corresponding to a machine, it's crucial to know with precision its geometry. In the case of the machine of Table 2.2, some dimensions and characteristics are going to be presented in this section. Table 3.2 obtained by Tommaso [20] shows the main constructive characteristics of the machine.

With these data and all the measurements made in the motor parts, some technical drawings could be made to detail each part.

Stator Dimensions

Once the rotor is going to be considered as a unique piece, the main measurements of interest are in the stator geometry are the internal and external diameter of the yoke, as well as the all the dimensions of the stator's teeth and slots. These measurements

Stator slots	36
Rotor bars	26
Stack length	159.55[mm]
Yoke's outer diameter	161.4[mm]
Yoke's inner diameter	132.78[mm]
Stator's inner diameter	104.2[mm]
Rotor's diameter	103.4[mm]
Air gap	0.4[mm]
Shaft's diameter	35.35[mm]
Ring length	7.9[mm]
Ring height	19.65[mm]

Table 3.2: Main characteristics of the motor's geometry

can be found in the Figs. 3-2, 3-3 and 3-4.

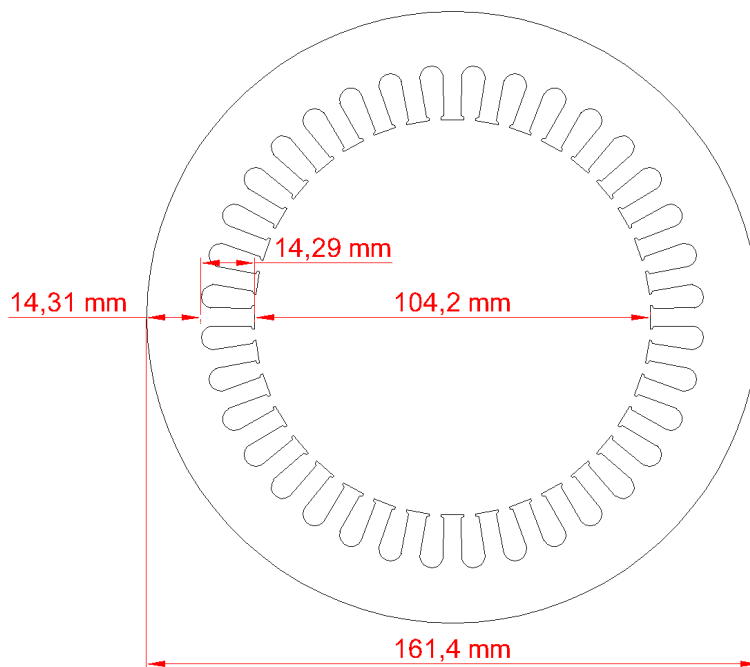


Figure 3-2: Technical drawing of the machine's stator yoke.

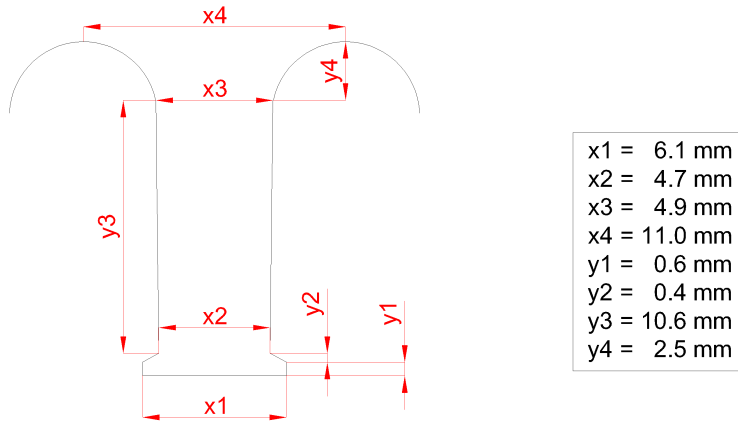


Figure 3-3: Technical drawing of the stator's teeth

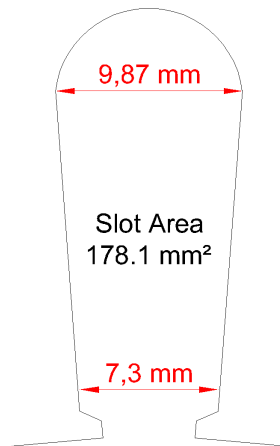


Figure 3-4: Technical drawing of the stator's slot

3.2.2 Thermal resistance between the frame and the ambient

$$(R_{th1})$$

R_{th1} is the thermal resistance between the frame and the ambient. In this model, this is the thermal resistance that will evacuate all the heat produced inside the machine by its losses. The main factors that influence in the calculation of R_{th1} are the frame and the fan design. The calculations, however may be very complex and not necessarily accurate because the geometry of the frame and fan can vary in many different ways. For that reason, its advisable that R_{th1} is measured instead of calculated. Once it deals with all the machine's losses and the frame temperature

is easy to be measured, there are no complications to calculate R_{th1} . When it's not possible to measure that temperature, it's convenient to assume a rated temperature rise of the frame. In the case of the motor of Table 2.2, a typical value would be 45K. Then R_{th1} is chosen accordingly. The calculation of the total power losses P_{loss} is important, because that value together with the average temperature rise θ_f of the frame will be used to calculate R_{th1} , like shown by Equation 3.7 [12].

$$R_{th1} = \frac{\theta_f}{P_{loss}} \quad (3.7)$$

3.2.3 Thermal resistance between the frame and the stator yoke (R_{th2})

Usually, the heat flow coming from the stator teeth is much larger than the heat generated internally in the stator yoke [12]. For that reason, the stator yoke is modeled as a single-node configuration. Peripheral and axial heat fluxes are neglected. This thermal resistance is given by Equation 3.8.

$$R_{th2} = \frac{\ln(r_2) - \ln(r_1)}{4\pi\lambda\ell} \quad (3.8)$$

In this case, r_1 is the radius defined at the top of the slots in the stator, and r_2 is the outer radius of the stator yoke, in contact with the frame, and ℓ is the length of the stator core.

3.2.4 Thermal resistance between the stator yoke and the stator teeth (R_{th3})

To get to the value of this resistance, the values of the stator's teeth geometry will be used. Also, it's necessary to define how the stator is seen from the point of view of a thermal network. These values, found in Fig. 3-3, are used in Equation 3.9 to determine this thermal resistance. R_{th3} , the thermal resistance between the stator yoke and the stator teeth is given by Eq. 3.9.

$$R_{th3} = \frac{1}{2} \left(\frac{\ln(r_2) - \ln(r_1)}{2\pi\lambda\ell} + R_0 \right) \quad (3.9)$$

where

$$R_0 = \frac{1}{\lambda Q_s \ell} \left[\frac{y_1}{x_1} + \frac{y_3}{x_3} + \frac{y_2}{x_1 - x_2} \left(\ln \left| \frac{x_1 \cdot y_2}{x_1 - x_2} \right| - \ln \left| y_2 - \frac{x_1 \cdot y_2}{x_1 - x_2} \right| \right) - \frac{\pi}{4} + \frac{a}{\sqrt{a^2 - 1}} \cdot \arctan \frac{a + 1}{\sqrt{a^2 - 1}} \right] \quad (3.10)$$

and

$$a = \frac{x_3 + 2y_4}{2y_4} \quad (3.11)$$

3.2.5 Thermal resistance between the stator teeth and the embedded windings (R_{th4})

This thermal resistance is calculated by Eq. 3.12.

$$R_{th4} = \frac{R_x R_y}{Q_s \ell (R_x + R_y)} \left(1 - \frac{R_{x0} R_{y0}}{720 R_x R_y} \right) \quad (3.12)$$

considering $\ell = \ell_{Fe}$, $d_a = 0.17-0.30$ mm and $\lambda_a = 0.03$.

The materials properties were used according with Appendix B . This approximation can bring good results with the simulation, but if the average stator winding temperature can be measured at the rated load, it's preferable to change R_{th4} in order to make the calculate average stator winding temperature match exactly the measured temperature.

3.2.6 Thermal resistance between the embedded windings and the end windings (R_{th5})

This thermal resistance in the circuit is R_{th5} . This resistance is considered separately because the winding has different temperatures in the embedded part and the part

that is outside the iron core. To model the temperature difference between these two parts of the windings, this thermal resistance is calculated like in Eq. 3.13.

$$R_{th5} = \frac{\ell}{Q_s A_{Cu} \lambda} \quad (3.13)$$

considering $\ell = \frac{l_{av}}{12}$, where l_{av} is the average conductor length of half a turn.

3.2.7 Thermal resistance between the rotor and the frame (R_{th6}), rotor and windings (R_{th7}), and between frame and end windings (R_{th8})

These three resistances are treated together, because to get to their values, some circuit analysis is needed, particularly, a wye-delta transformation, like shown in Fig. 3-5.

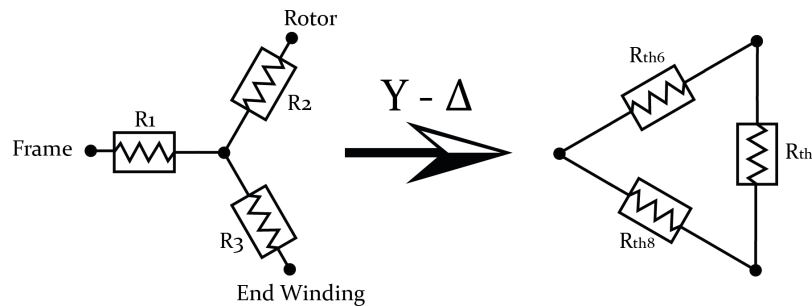


Figure 3-5: Y- Δ transformation. It eliminates one node in the thermal circuit.

So, for the thermal circuit, based on the motor parameters, R_1 , R_2 and R_3 are calculated. Then, the Y- Δ conversion is made. The relations for the heat transfer coefficients to get these three thermal resistances are basically empirical [12]. It's important to observe that the resulting thermal resistances have to be divided by two, because the heat paths at the drive side and the fan side are in parallel. The equations that define these three resistances give the respective heat transfer coefficient of each. The unit of the coefficient α is W/m²K. So, by dimension analysis, from the power transfer equation, can be concluded that the resistance value will be:

$$R = \frac{1}{Area * \alpha} \quad (3.14)$$

R_1 is the resistance between the frame and the internal air. To get its value, Eq. 3.15 is used, and the considered area is the sum of the internal end shield area and the internal frame area.

$$\alpha_{R1} = k_1 + k_2 u_r^{0.65} \quad (3.15)$$

where $k_1 = 15 \text{ W/m}^2\text{K}$ and $k_2 = 6.75 \text{ (s/m)}^{0.65} \text{ W/m}^2\text{K}$.

The value of R_2 , the resistance between the rotor and the internal air, is given by Eq. 3.16, that is:

$$\alpha_{R2} = k u_r^{0.65} \quad (3.16)$$

where $k = 16.5 \text{ W(s/m)}^{0.65}/\text{m}^2\text{K}$ and u_r is the peripheral speed of the rotor. The area associated with the heat transfer coefficient is calculated by

$$A = 2bhn + \pi r \delta^2 \quad (3.17)$$

where b and h are respectively the length and the height of the rotor fins, and n is the number of fins.

The resistance R_3 , between the stator end winding and the internal air, has the following heat transfer coefficient, given by Eq. 3.18. The considered area is the total area of the end winding.

$$\alpha_{R3} = k_1 + k_2 u_r^{0.6} \quad (3.18)$$

where $k_1 = 6.5 \text{ W/m}^2\text{K}$ and $k_2 = 5.25 \text{ W(s/m)}^{0.6}/\text{m}^2\text{K}$. In this case, α includes already the radiation effect between the end winding and the shield.

To perform the Y- Δ , transformation, the following equations are used, respect to the resistances shown in Fig. 3-5:

$$R_{th6} = \frac{R_1 R_2 + R_2 R_3 + R_3 R_1}{R_3} \quad (3.19)$$

$$R_{th7} = \frac{R_1 R_2 + R_2 R_3 + R_3 R_1}{R_1} \quad (3.20)$$

$$R_{th8} = \frac{R_1 R_2 + R_2 R_3 + R_3 R_1}{R_2} \quad (3.21)$$

3.2.8 Thermal resistance between the rotor and the stator teeth (R_{th9})

The resistance between the rotor and the stator teeth is R_{th9} , and it's calculated by using Eqs.

$$\alpha_{R_{th9}} = \frac{Nu \lambda_f}{2\delta} \quad (3.22)$$

$$R_{th9} = \frac{1}{2 \pi r \delta \ell (\alpha_{R_{th9}})} + \frac{R_0}{2} \quad (3.23)$$

where R_0 is calculated by Eq. 3.10, $Nu = 2$, and the values for $\ell = \ell_{Fe}$, λ_f can be found in Appendix 2. For simplicity reasons, the air gap thermal expansion was neglected.

3.2.9 Thermal resistance between the rotor and the bearings (R_{th10})

R_{th10} is the thermal resistance between the rotor and the bearings. It consists of four parts that should be summed together. These four values will be called from $R_{th10.1}$ to $R_{th10.4}$. The first of them is the one of the rotor yoke. It's defined by

$$R_{th10.1} = \frac{\ln r_2 - \ln r_1}{2 \pi \lambda \ell} \quad (3.24)$$

where r_2 is the radius to the bottom of the rotor slots, r_1 is the shaft radius and λ is the thermal conductivity of the core material, and $\ell = \ell_{Fe}$.

The second part of R_{th10} is the thermal contact resistance between the rotor core and the shaft. This value is difficult to give with reasonable precision, because it depends on the contact pressure. Empirically, it is known that this value is close to the one given by Eq. 3.24 [12], and so the same value will be used in the calculations.

The third part of R_{th10} regards the thermal resistance through the shaft. It is given by

$$R_{th10.3} = \frac{\ell}{\pi r^2 \lambda} \quad (3.25)$$

where ℓ is the distance between the rotor center and the bearings. The fourth part ($R_{th10.4}$) is equal to R_{th11} .

3.2.10 Thermal resistance between the bearings and the frame (R_{th11})

R_{th11} , the thermal resistance between the bearings and the frame is given by

$$R_{th11} = 0.25 \cdot k_1(0.12 - k_2 d_b)(33 - k_3 \omega d_b) \quad (3.26)$$

where $k_1 = 0.45$ K/W, $k_2 = 1$ m⁻¹ and $k_3 = 1$ s/m. In the simulation, the rated value of ω was used.

3.3 Simulation Results for the thermal circuit

The circuit proposed by [12], and presented in this chapter was implemented in Simulink[®], and the results presented in this section. The simulation was made considering the rated parameters of the motor, in Table 2.1. The values found for the thermal resistances of the circuit in Fig. 3-1 were the ones indicated in Table 3.3

The results of the simulation of the induction motor with this thermal network are shown in Table 3.4. The simulation was performed with the model of the induction

Resistance	Value (K/W)
R_{th1}	0.0673
R_{th2}	0.0057
R_{th3}	0.0121
R_{th4}	0.0531
R_{th5}	0.0579
R_{th6}	2.2814
R_{th7}	10.9471
R_{th8}	1.4612
R_{th9}	0.3227
R_{th10}	1.8911
R_{th11}	0.2062

Table 3.3: Values of thermal resistances calculated for the modeled motor

	Frame [°C]	Stator Yoke [°C]	Stator Teeth [°C]	Interior Windings [°C]	End Windings [°C]	Rotor [°C]	Bearings [°C]
Simulation Results	62.0	64.9	70.3	88.4	95.5	94.0	65.2
Reference Paper	61.6	64.3	72.6	94.2	101.4	119.0	72.2

Table 3.4: The values of temperature for the motor modeled in this work are compared with a different motor of the same rated power, used in the reference paper [12].

motor with iron losses, iron saturation and resistances changing with the temperature. The results shown in 3.4 are for the steady-state temperatures in these conditions. The simulation was performed with the motor running in direct start, connected to the grid, and with rated load.

These results show that even with a simplified model like the one used in this chapter, good approximations can be made to the real temperature of the motor. In [12], it's possible to see that this model also offers good approximations to transient temperatures.

The thermal model of the induction machine offers the possibility of having a more complete simulation model. In the real machine, as the temperature changes, the electrical parameters of the motor also change, mainly the resistances. If the

motor's temperature is not taken into account, the real value of the resistances will differ from the ones used in simulation (and in the control). It can lead to the implementation of less efficient controllers.

The model with variable resistances also offers the possibility of trying algorithms for tracking the real value of these resistances, that can be implemented in real motors. Some of these algorithms are going to be explained and tested in the next chapter.

Chapter 4

Online Parameters Estimation

In this chapter, the induction motor's model developed so far will be put to test some different online parameter estimation methods. The idea of these methods is that the machine's parameters can be estimated in real time, and updated in the control, making it more efficient, and less vulnerable to temperature and saturation effects. First, the main concepts of online parameters will be explained, and then some techniques will be presented and discussed, and then finally some simulations will show how these algorithms work and how they can improve the controllers by re-tuning them with the actual real-time values of the machine's parameters.

4.1 Importance and Main Concepts

The control of an induction machine requires the knowledge of some of its physical parameters. A robust controller needs the values of at least some of the motor's parameters with precision, as the controller is tuned with different parameters depending on the plant it is going to control. If the parameters are not known, it will work in detuned operation, having unexpected overshoots, settling times, or even instability. The same way a controller with wrong parameters is detuned, it may also become not perfectly tuned when these parameters change, as it is the case of resistances and inductances, because of temperature and saturation, respectively (the inductance also changes with the temperature, but in the temperature range of an induction motor,

this change is not significant).

One good example of problem caused by parameters mismatches is when the controller uses rotor flux oriented control. These mismatches will cause that the actual position of the rotor flux doesn't coincide with the position assumed by the controller, so it won't be able to perform a decoupled control of torque and flux. This situation is illustrated by Fig. 4-1.

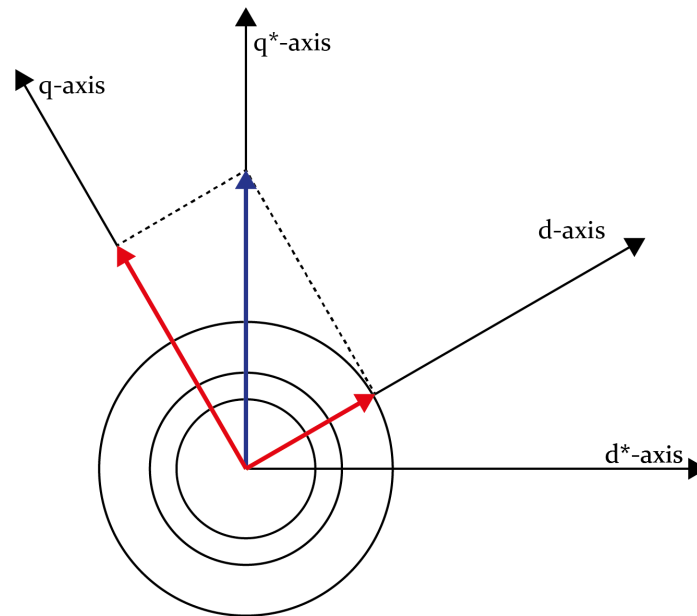


Figure 4-1: Effect of detuned parameters in the commands applied by the controller. dq^* -axis assumed by the controller in the rotor field oriented control differ from the real position.

The actual rotor flux has the d- and q-axis component, and the parameter's mismatch takes the controller to assume that these axes are in the positions d^* and q^* . So, when the controller gives, for instance, a current command aligned with the q^* -axis, to control torque (indicated by the blue vector), in reality, this command will have a component in the real d-axis and in the real q-axis (red vectors), not affecting only torque, but also flux. So, the study of methods to mitigate this problem can be a real positive impact in the robustness of the controller for the induction machine.

4.2 Main Parameter Estimation Techniques

The techniques for parameter estimation can be divided into two major groups: offline and online parameter estimation methods [25]. This work focus in the online methods, and so the offline methods won't be discussed, assuming that the initial parameters of the induction machine are known at the beginning. There are several techniques used to estimate the machine's parameters online, but this work will go through spectral analysis, observer-based and Model Reference Adaptive System-based techniques, as indicated in Fig. 4-2.

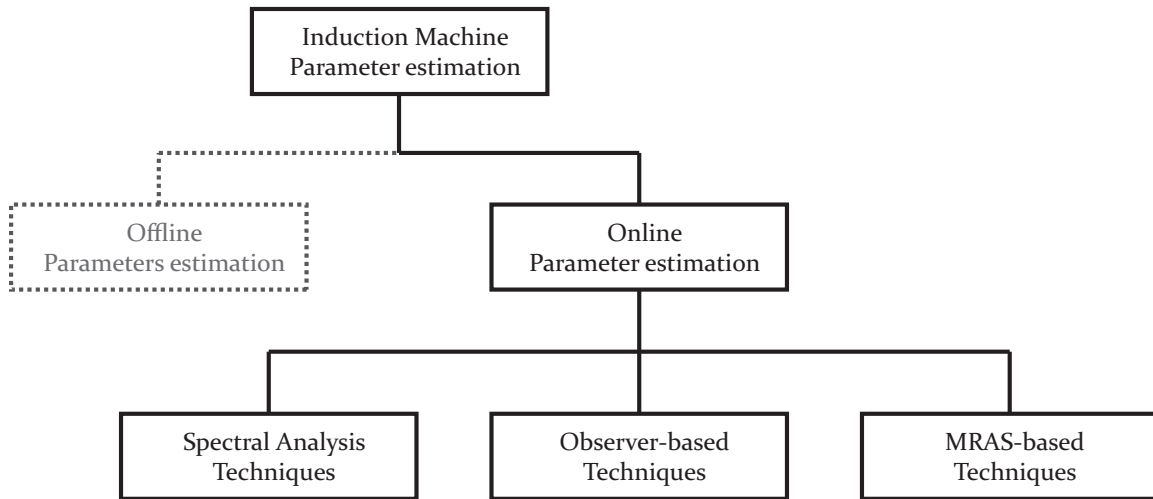


Figure 4-2: Schematic resume of the methods reviewed in this work.

4.2.1 Spectral Analysis Techniques

This group of methods comprise all the cases where the online identification is based on the measured response to a deliberately injected test signal or an existing characteristic harmonic in the voltage/current spectrum [25]. After the injection of these signals, the stator's currents and/or voltages are sampled and their spectrum is analyzed. Many different articles explore this technique, like [18], where it is proposed to inject negative sequence components. An online technique for determining the value of the rotor resistance by detecting the negative sequence voltage is proposed in that article.

One important information when taking this kind of method is if the motor is being used as torque drive. In that case, extra caution has to be taken to avoid torque pulsations. If that happens, the torque controller may try to cancel that disturbance, preventing it from being injected into the system.

If the main drawback of this method is the possible torque pulsations when a disturbance signal is injected in the current, some methods also try to overcome that problem injecting the disturbances in the d-axis current. That current affects only flux, and not the torque, like proposed in [24]. The problem is that the parameter estimation can't be 100% correct, and in that case, there will always be some coupling between d and q currents, what would cause some torque pulsation.

Because of the purpose of this work, that is aimed to traction applications, these methods are not of special interest.

4.2.2 Observer-based Techniques

Observer-based techniques don't require the injection of any disturbance to the system. Some of the techniques use the tuning of an extended Kalman filter (EKF) for parameter estimation, like the ones proposed in [14] and [15].

In these cases, one disadvantage is that, the full-order EKF is computationally very heavy if compared with reduced order-based systems.

Also the extended Luenberger observer (ELO) has been used for estimating parameters online, and [6] provides a comparison from the operation point of view between the EKF and the ELO.

As an overall observation, the main problems related to EKF and ELO applications are regarding the computational intensity needed by these methods. Also, the fact that all the inductances are considered constants in the motor equations. In this case, once this work aims to estimate resistances and inductances, this method is also not the best option among the considered ones.

4.2.3 Model Reference Adaptive System-Based Techniques

This third group of online parameter estimation methods is based on model reference adaptive control. The main advantage of these methods is the simplicity to implement them, requiring less computational resources. To summarize the idea of the MRAS, through this methods one quantity is calculated in two different ways. One of them with parameters and references inside the control system. The second is calculated from values that can be measured. One of these two models is independent of the rotor resistance. So, the difference between the two results is used as an error signal. The control (Usually a PI controller) considers that this difference is due only to the rotor resistance, and changes its value until the error signal is zero.

There are many different models that use this method, and the efficacy of each method, obviously depends on the accuracy of each model. The main difference between the different methods is which is the quantity selected for adaptation purposes. One of the most applied approaches in MRAS methods are the reactive power-based ones. Other possibilities are the selection of torque, rotor back-EMF, rotor flux magnitude, rotor flux d- and q-components, etc. [25].

The main drawback of this group of methods is the impossibility to adapt values at zero speed and zero load torque.

4.2.4 Other Methods

Besides the methods presented so far, there are many others in literature that could be used to make online estimation of the induction motor's parameters. The method presented in [23], for instance, doesn't use test signals or complex computations that could need extensive DSP's resources. The method is based on a special switching technique of the PWM inverter, current regulated. That way, it allows the measurement of the induced voltage across the disconnected stator phase, so the rotor time constant is directly identified.

Also, in the more recent years, different methods propose the use of artificial intelligence (AI), and specifically neural networks for online rotor time constant esti-

mations. Also fuzzy logic has been used.

4.3 Model Reference Adaptive System Applied to Parameter Estimation

From the methods explained above, the one chosen for making the simulations and to be applied for the purpose of this work was the Model Reference Adaptive System-based (MRAS method). The basic scheme of the MRAS method is presented in Fig. 4-3.

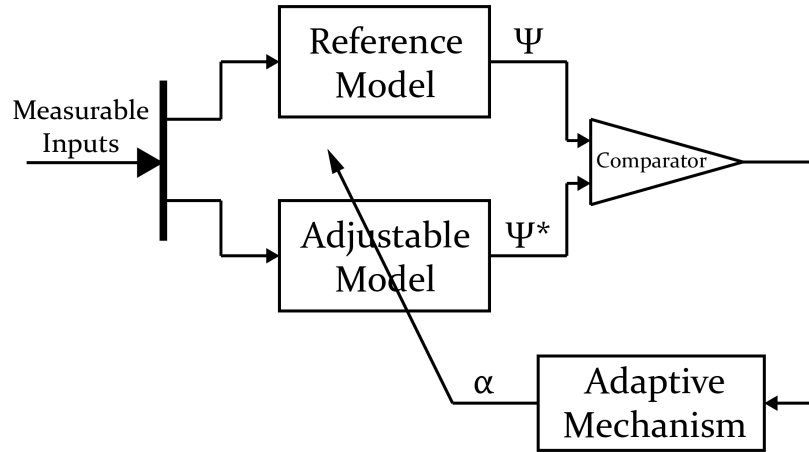


Figure 4-3: MRAS: The reference model should be independent of α , while the adjustable model depends on it. From the two models, Ψ is obtained and compared. The difference is used to adapt the value of α in the adjustable model.

4.3.1 Estimation's Design

The estimator used takes the theory of Indirect Field Oriented Control (IFOC) for IM drives, derived from the current model of the rotor flux, given as:

$$\dot{\varphi}_{ri} = L_m \alpha_r i_s - \alpha_r \varphi_{ri} + j \omega_r \varphi_{ri} \quad (4.1)$$

where φ_{ri} is the rotor flux vector, calculated by the current model of the induction motor, ω_r is the rotor's speed, and α_r is the rotor natural frequency, or $1/\tau_r$.

If all the parameters used in this equation were precisely known, the rotor flux could be exactly calculated with no errors. However, in real applications, the rotor's resistance is a changing value, and its value changes depending mainly on the temperature in the rotor, for ohm thermal effect. Considering that the value of the rotor's resistance is not known, but estimated, equation 4.1 could be rewritten as:

$$\dot{\hat{\varphi}}_{ri} = L_m \hat{\alpha}_r i_s - \hat{\alpha}_r \hat{\varphi}_{ri} + j\omega_r \hat{\varphi}_{ri} \quad (4.2)$$

The Estimation of R_r

A consequence of Eq. 4.2, can be observed in Fig. 4-4.

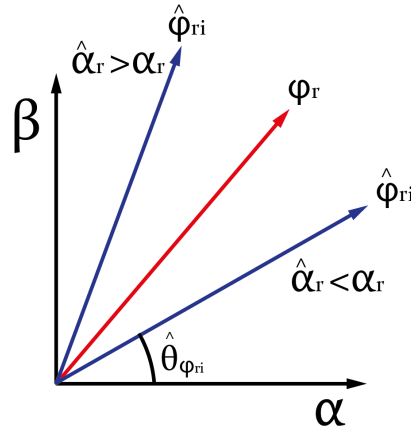


Figure 4-4: Rotor flux obtained from the current model

If the estimated value of α is greater than the real value, the estimated rotor flux vector ($\hat{\varphi}_{ri}$) will lead the actual rotor flux vector (φ_r), and if $\hat{\alpha}$ is smaller than α , $\hat{\varphi}_{ri}$ will lag φ_r .

Taking that into account, if the value of the rotor flux is φ_r , the phase shift between $\hat{\varphi}_{ri}$ and φ_r can be obtained making the cross-product between the two vectors, like in equation 4.3

$$\sin(\theta_{\varphi_{ri}}) = \frac{\varphi_r \times \hat{\varphi}_{ri}}{|\varphi_r| \times |\hat{\varphi}_{ri}|} \quad (4.3)$$

where θ is the phase-shift between the estimated and the reference fluxes. That way, considering that the rotor time constant is the only factor with influence in the

phase-shift between the estimated and the real fluxes, the phase-shift can be used to estimate \hat{R}_r . This idea is schematized in Fig. 4-5.

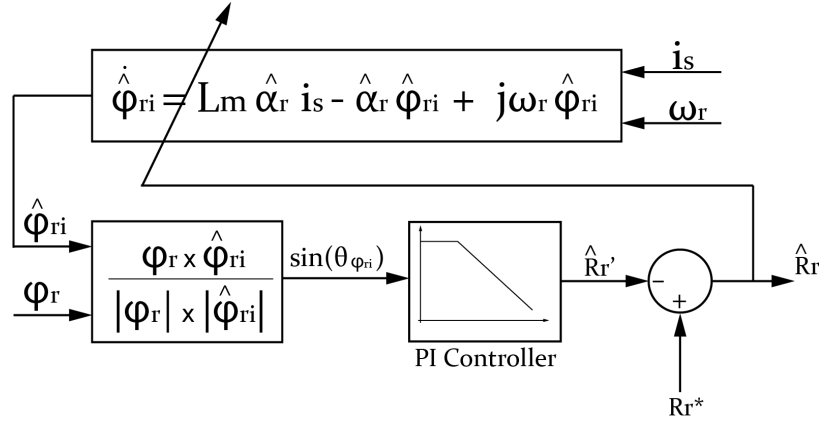


Figure 4-5: Estimation of the rotor resistance from the phase-shift between the real rotor flux and the estimated rotor flux.

In Fig. 4-5, ”*” accounts for nominal values of the parameters. Also, another important observation is that this method counts with the real flux φ_r as an input. The way to obtain it will be discussed later in this work.

The estimation of L_m

In traction applications, the flux level in the machine changes very often, depending on the state of operation. With the change in the flux levels, the mutual inductance also changes. Similarly to the rotor resistance R_r , the mutual inductance L_m is also in the equation of the current model. Eq. 4.1. It means that any change in \hat{L}_m would cause a change in $\hat{\varphi}_{ri}$ that would also deviate from the real value. One advantage of this method is that the value of R_r is got from the phase error of $\hat{\varphi}_{ri}$, and so with a good design of the closed-loop system, the phase error will be corrected to 0 (and R_r will be correctly estimated) even if the estimation of \hat{L}_m is no correct. The effect of the error in \hat{L}_m can be seen in Fig. 4-6.

In Fig. 4-6, in the beginning of the simulation, both \hat{R}_r and \hat{L}_m are correctly estimated. As a consequence, $\hat{\alpha}_r$ is also correctly estimated. In the simulation time $t = 0.5s$, an error is deliberately introduced in the estimation of R_r , and consequently $\hat{\alpha}_r$ reflects that error. In simulation time $t = 1s$, the estimation control of Fig. 4-5 is

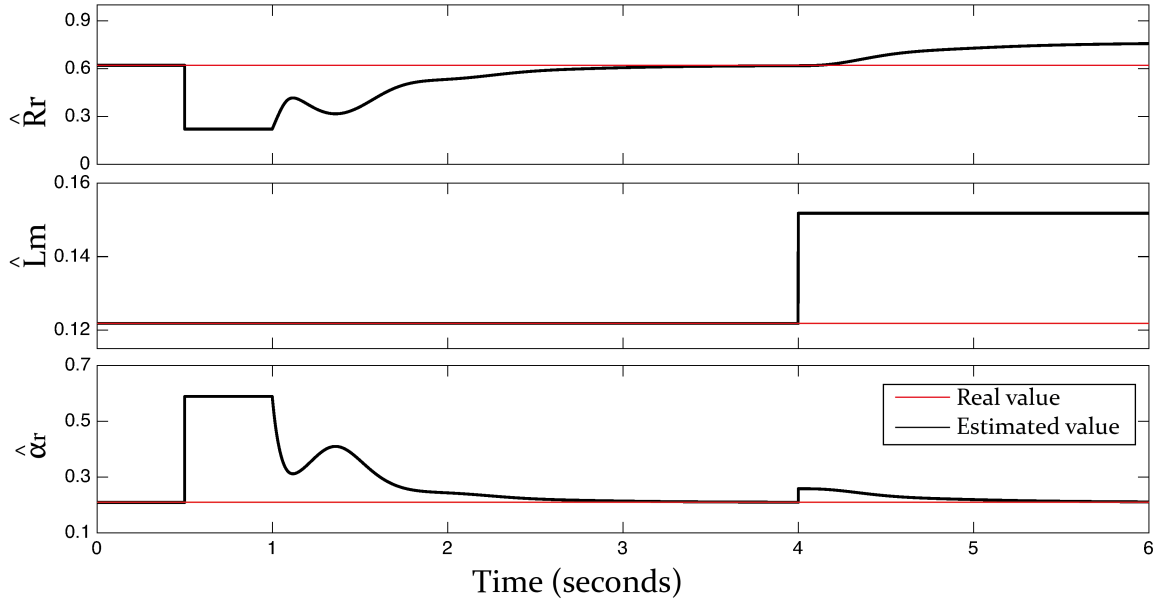


Figure 4-6: Operation of the closed-loop control in the correction of $\hat{\alpha}_r$

activated, and the values of \hat{R}_r and $\hat{\alpha}_r$ are corrected. In $t = 4\text{s}$, an error is introduced in the value of L_m . This error causes the instantaneous deviation of $\hat{\alpha}_r$ and the control brings it back to the real value, however, R_r gets detuned, being higher than the actual value. From Fig. 4-6 we can conclude that in fact, the phase error of $\hat{\varphi}_{ri}$ is dependent only on the rotor-time constant $\hat{\tau}_r$.

Once this control is implemented in a phase-error driven closed-loop system, it forces \hat{R}_r to change its value, compensating the error in \hat{L}_m , so $\hat{\tau}_r$ can be indirectly corrected. Although $\hat{\tau}_r$ is corrected this way, neither \hat{R}_r or \hat{L}_m are corrected. This is

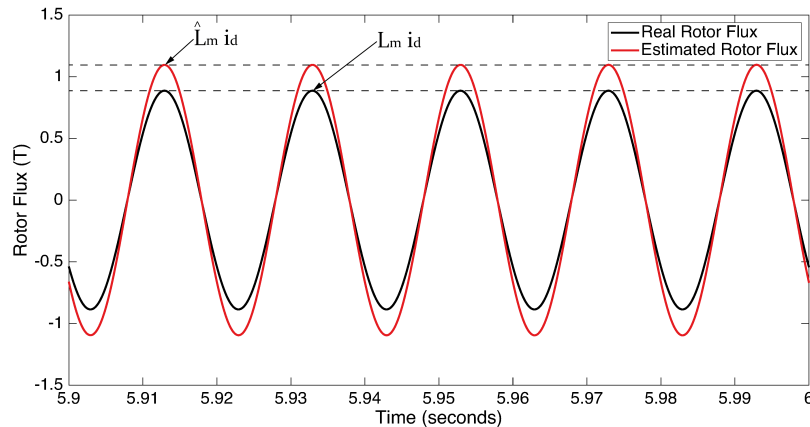


Figure 4-7: Mismatch in the flux magnitude after the correction of $\hat{\alpha}_r$

why \hat{L}_m needs to be estimated and corrected too.

Fig. 4-7 shows what happens when the value of \hat{L}_m is not properly corrected. Once the flux is the product of the mutual inductance by the current, if the mutual inductance is not correctly estimated, the estimated flux won't be also. In this figure it's possible to observe that the magnitude of $\hat{\varphi}_{ri}$ is still greater than the actual value of the rotor flux, even though the phase error was corrected. Also, the magnitude error between $\hat{\varphi}_{ri}$ and the actual value is proportional to the mismatch between \hat{L}_m and L_m for any magnetizing current. These facts lead us to the following conclusions about this parameter estimation method:

Even with the estimated flux ($\hat{\varphi}_{ri}$) and the actual flux (φ_{ri}) totally aligned and with no phase error, by the estimation technique presented in Fig. 4-5, if the value of L_m is not known, it has to be estimated too in order to obtain a precise value of R_r . Knowing that the mismatch between L_m and \hat{L}_m is reflected to the mismatch between $\hat{\varphi}_{ri}$ and φ_{ri} , the value of \hat{L}_m can be corrected by referring to the magnitude deviation [27]. From that idea, the estimation diagram shown in Fig. 4-5 can be updated to the one shown in Fig. 4-8, where \hat{R}_r and \hat{L}_m are estimated in parallel, at the same time.

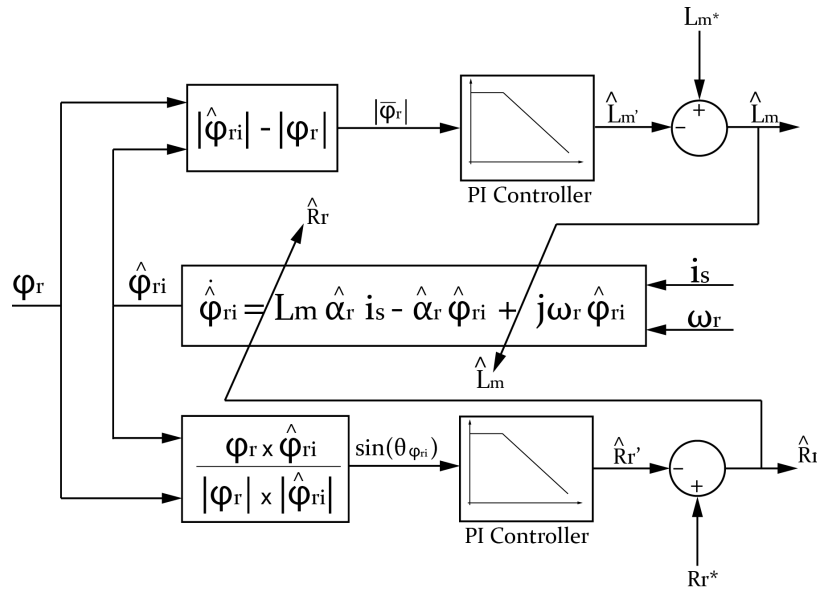


Figure 4-8: Simultaneous estimation of the rotor resistance and the magnetizing inductance

Controllers' Dynamics

One important observation is that one of the inputs of this method is the real rotor flux. This is a measurement that is not common in real applications, what makes this method very difficult to implement. In the next section, some methods to obtain that flux will be discussed. For the description of the estimation methods mentioned previously in this chapter, this model constitutes a Model Reference Adaptive System, with the real flux as the reference model, and the current model of the rotor flux as the adaptive one. The PI controllers constitute the adaptive mechanism.

Equations 4.4 and 4.5 give the dynamics of the magnitude and phase of the rotor flux [27].

$$\dot{\theta}_{\varphi_{ri}} = \omega_r + \frac{1}{|\varphi_{ri}|} \frac{L_m}{L_r} R_r i_{sm} \sin(\theta_{is} - \theta_{\varphi_{ri}}) \quad (4.4)$$

$$|\dot{\varphi}_{ri}| = -\frac{R_r}{L_r} |\varphi_{ri}| + \frac{L_m}{L_r} R_r i_{sm} \cos(\theta_{is} - \theta_{\varphi_{ri}}) \quad (4.5)$$

So, from these equations of the dynamics of the angle and magnitude of the flux, the adaptive mechanisms can be obtained. To make it simpler, in Eq. 4.6, R_r is considered the only parameter to be adapted, and the effect of a possibly detuned L_m is not considered on the flux phase $\hat{\theta}_{\varphi_{ri}}$. The same way, in Eq. 4.7, L_m is considered the only parameter to be adapted, and the effect of a possibly detuned R_r is not considered on the flux magnitude $|\hat{\varphi}_{ri}|$. Taking these assumptions into account, these two equations can be rewritten as

$$\dot{\hat{\theta}}_{\varphi_{ri}} = \omega_r + \frac{1}{|\varphi_{ri}|} \frac{L_m}{L_r} \hat{R}_r i_{sm} \sin(\theta_{is} - \hat{\theta}_{\varphi_{ri}}) \quad (4.6)$$

$$|\dot{\hat{\varphi}}_{ri}| = -\frac{\hat{R}_r}{L_r} |\hat{\varphi}_{ri}| + \frac{\hat{L}_m}{\hat{L}_r} R_r i_{sm} \cos(\theta_{is} - \theta_{\varphi_{ri}}) \quad (4.7)$$

The dynamics from mismatches of R_r and L_m to the resultant changes in $\hat{\theta}_{\varphi_{ri}}$ and $|\hat{\varphi}_{ri}|$, used to tune the PI controllers are [27]:

$$\dot{\hat{\theta}}_{\varphi_{ri}} = \frac{i_{sm}}{|\varphi_{ri}|} \frac{L_m}{L_r} [-R_r \cos(\theta_{is} - \theta_{\varphi_{ri}}) \bar{\theta}_{\varphi_{ri}} + \bar{R}_r \sin(\theta_{is} - \theta_{\varphi_{ri}})] \quad (4.8)$$

$$|\dot{\hat{\varphi}}_{ri}| = -\alpha_r |\bar{\varphi}_{ri}| + \bar{L}_m \frac{1}{L_r} \alpha_r |\varphi_{ri}| \quad (4.9)$$

where $\bar{\theta}_{\varphi_{ri}} = \hat{\theta}_{\varphi_{ri}} - \theta_{\varphi_{ri}}$, and $|\bar{\varphi}_{ri}| = |\hat{\varphi}_{ri}| - |\varphi_{ri}|$ represent the deviations of the estimated values.

So, the plants in the two estimation loops for \bar{R}_r and \bar{L}_m can be expressed respectively as:

$$G_p R(s) = \frac{\bar{\theta}_{\varphi_{ri}}}{R_r} = \frac{\sin(\theta_{is} - \theta_{\varphi_{ri}})}{\frac{|\varphi_{ri}|}{|i_s|} \frac{L_r}{L_m} p + R_r \cos(\theta_{is} - \theta_{\varphi_{ri}})} \quad (4.10)$$

$$G_p L(s) = \frac{|\bar{\varphi}_{ri}|}{\bar{L}_m} = \frac{\alpha_r |\varphi_{ri}| / L_r}{p + \alpha_r} \quad (4.11)$$

It's important to observe that the gain in Eq. 4.10 depends on the machine's operation mode. It's positive for motoring mode and negative for generating mode [27].

4.3.2 Observation of the Rotor Flux

As commented before, in the method seen so far, to obtain a good performance of the estimations, the rotor flux has to be precisely obtained, once it is an input to the MRAS adaptive system. However it is known that the rotor flux is a magnitude that is hard to be measured. There are many different proposed methods to estimate, or observe the rotor flux, like the one proposed in [5] that uses a closed-loop flux observer based on the current estimation error, with a sliding mode function. Also, open-loop flux observers are widely used in the control of induction machines.

Open-Loop flux observers

Among the open-loop observers, there are three basic topologies [10], dictated by the measured states/inputs and corresponding flux model. Two of them are reduced order

models, named "current model" and "voltage model". The third one is a full-order observer, with respect to the induction machine electrical model. Also, we can cite a fourth observer based on cancellation methods.

- The current model can be defined by equation 4.1, already used in this chapter.
- The voltage model can be defined by Eq. 4.12.

$$\varphi_{rv} = \frac{L_r}{L_m} \varphi_s - \frac{\sigma}{1 - \sigma} L_m i_s \quad (4.12)$$

where

$$\sigma = 1 - \frac{L_m^2}{L_r L_s} \quad (4.13)$$

and φ_s is the stator flux, denoted by

$$\dot{\varphi}_s = V_s - R_s i_s \quad (4.14)$$

- The full order open-loop flux observer is derived directly from the induction machine electrical model, characterized by equations from Eq.2.16 to Eq. 2.23.

- The cancellation method is an open-loop flux estimator based on the rotor and stator flux linkage and voltage loop equations [10].

Closed-loop flux observers

Closed-loop rotor flux observers can use some of the open-loop models and be developed directly from the induction machine model. One method, described in [10], uses the concept that measuring the stator voltage allows the stator current to be estimated and compared to the measured current. The rotor flux is used as feedback on the stator current, so the current error is driven to zero by using corrective feedback over the estimated rotor flux. Ideally the rotor flux estimate converges on the correct value when the current error goes to zero.

Also, some techniques of closed-loop observers use sliding mode observers, like the ones used in [5] and [27].

4.4 Simulation Results

Measured Flux as Reference

After getting to the MRAS model of Fig. 4-8, that allows the simultaneous estimation of R_r and L_m , and also checking the dynamics of the system to design the controllers, a simulation can be performed with the modeled induction machine to simultaneous estimation of these parameters. For the first simulation, no reference model was used. Instead, the rotor flux was directly got from the motor model and put as input to the adaptive system. That would be the ideal case, because if the flux could be measured, any error would be discarded. The results of this first simulation are shown in Fig. 4-9. In this simulation, both parameters values change at time $t = 0.5s$. At $t = 1s$, the resistance tracking algorithm is activated and it begins to track the real value of the resistance. At time $t = 8s$, R_r stabilizes at the value of 1Ω , and the estimated value gets to it with no steady-state error. Also for the estimated inductance, the steady-state error is equal to zero.

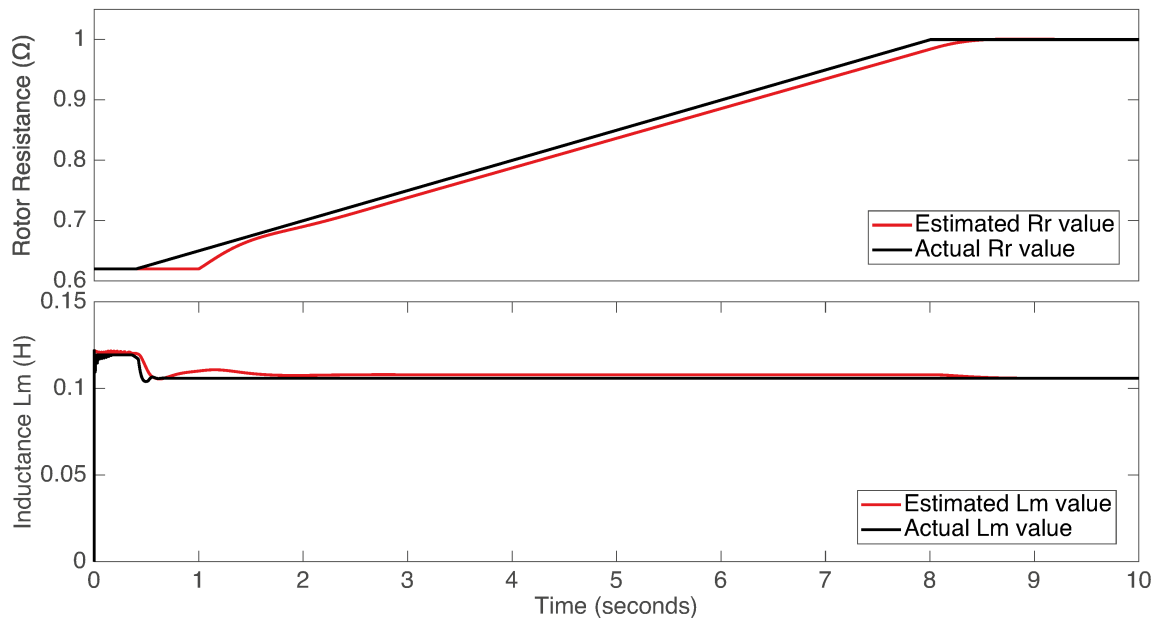


Figure 4-9: Parallel estimation of R_r and L_m - Measured flux as reference.

4.4.1 Open Loop Voltage Model as Reference

The second simulation made for the parameter estimation algorithm was putting the motor voltage model (Eq. 4.12 to Eq. 4.14) as reference for the block diagram of Fig. 4-8. In this case, as mentioned in the previous section, the flux is an approximation of the real flux, and when the parameters change, the reference model becomes slightly different from the real flux. This difference is translated into some steady-state error in the estimation, as it can be observed in Fig. 4-10.

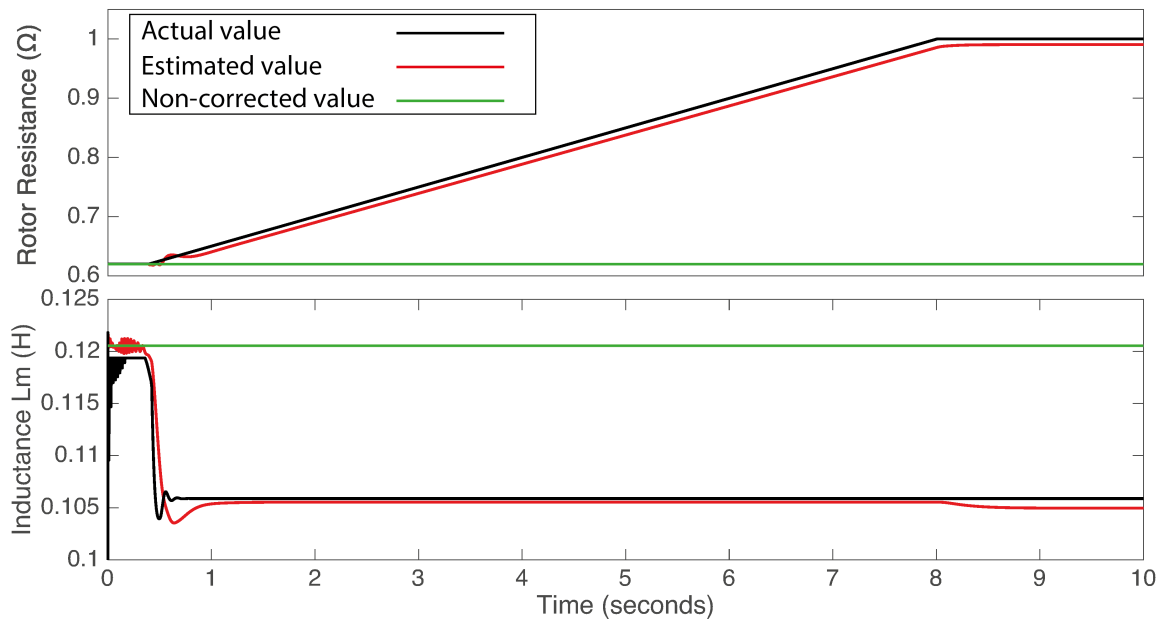


Figure 4-10: Parallel estimation of R_r and L_m - Open loop voltage model as reference.

In this figure, the steady-state error can be observed, however, if the values are compared, the error is so much smaller than the error obtained if the no correction were applied to the estimated values. It can be assessed numerically in the data of Table 4.1.

	Rotor	Magnetizing
	Resistance (Rr)	Inductance (Lm)
Estimated Value Error	0.95 %	0.85%
Non-corrected value Error	38%	14.3%

Table 4.1: Steady-state error with and without online parameter estimation for the simulation of Fig. 4-10.

So, from these simulations, it's possible to conclude that the parallel estimation of R_r and L_m brings considerably good results, with a reasonable approximation of the real parameters, and it can be used as a good option to retune the controllers parameters and make the machine control more efficient.

Chapter 5

Conclusion

In this work a very complete and multi-domain model of the induction machine was implemented and simulated.

Beginning by the equivalent circuit to analyze the steady-state response of the model, observing the influence of the iron losses equivalent resistance in that circuit, and then going to a dynamic model.

Despite the fact that there are many different methods to implement that dynamic model, as discussed in Chapter 2, the one implemented was demonstrated to be an accurate model, representing with good fidelity the behavior of the a real induction machine.

The addition of the thermal model, topic approached in Chapter 3, gives to the whole model a new level of accuracy, allowing different research lines. The thermal model includes a new domain that interacts with the electrical part, changing the value of the resistances depending on temperature, a phenomenon that happens in real machines, and is often ignored in the most of the simulation models of commercial softwares.

Chapter 4 made use of the models implemented in Chapters 2 and 3 to study a very useful technique in the control of induction machines. Thanks to the multi-domain model implemented, it was possible to verify that with a very simplified online parameter estimator, it's possible to significantly reduce the error between the real parameters and the ones used to tune the controllers.

5.1 Future Work

All the simulations made in this work had as input voltage source an ideal sinusoidal three-phase generator. In the future work, the same model will be used and tested being driven by power converters. The use of these converters bring new challenges in the run towards efficiency and power quality.

Also, instead of only estimating the parameters, with the multi-domain model it's possible to develop a research on estimating the temperature based on the parameters.

Appendix A

Matlab Source Code for Induction Motor Equivalent Circuit Analysis

```
%Here go the Motor parameters:  
  
P = 4; %Number of Poles  
f = 50; %Frequency [Hz]  
  
R1 = 1.1; %Stator Resistance [Ohms]  
R2 = 0.67; %Rotor Resistance [Ohms]  
Lls = 0.0077; %Stator leakage inductance [H]  
X1 = 2*pi*f*Lls; %Stator Leakage Reactance [Ohms]  
Llr = 0.0077; %Rotor leakage inductance [H]  
X2 = 2*pi*f*Llr; %Rotor leakage Reactance [Ohms]  
Lm = 0.1218; %Magnetizing inductance [H]  
Xm = 2*pi*f*Lm; %Magnetizing Reactance [Ohms]  
Rm = 1500; %Core losses equivalent resistance [Ohms]  
s = 2.1/100; %slip [%]  
B = 1e-4; %Friction damping coefficient
```

```

Vin = 400/sqrt(3); %Phase Voltage RMS [V]

%=====
%MECHANICAL CALCULATIONS
wmRPM = 120*f/P*(1-s); %RPM - Synchronous mechanical speed
wmRAD = 2*pi*wmRPM/60*(1-s); %rad/s - Synchronous mechanical speed

% CALCULATING THE EQUIVALENT IMPEDANCE OF THE MOTOR:

imp3 = R2/s + 1i*X2; %rotor elements
imp2 = (Rm*1j*Xm)/(Rm + 1j*Xm); %Magnetizing elements
imp1 = R1 + 1j*X1; %stator elements
eqImp = imp1 + (imp2*imp3)/(imp2 + imp3);
%=====
% CALCULATING THE RESULTING CURRENT

iInput = Vin/eqImp; %Input Current [A]
[ang,Current] = cart2pol(real(iInput),imag(iInput));
angDeg = 180*ang/pi;
%=====
%MOTOR INPUT APPARENT POWER:

Sin = abs(3*Vin*iInput); %VA
Pin = real(3*Vin*iInput); %W

%=====
% LOSSES
E2 = Vin - iInput*(R1 + X1); %Voltage in the magnetizing branch
I2 = E2/imp3;

```

```

Pstator = 3*R1*Current^2; %Losses in the stator winding [W]

Pg = abs(3*I2^2*(R2/s)); %Power in the Airgap [W]

Protor = real(3*R2*I2^2); %Losses in the rotor [W]

ironLosses = real(3*(E2^2)/Rm); %Iron Losses [W]

frictionLosses = B*wmRAD^2; %Friction Losses [W]

Pmec = Pg - Protor - friction Losses; %Power available in the rotor

Torque = Pmec/wmRAD; %N.m

Effic = Pmec/Pin; %Efficiency

fprintf('The rated speed of this machine is %.2f RPM\n', wmRPM);
fprintf('The rated mechanical power for this machine is %.2f kW\n',
    ↪ Pmec/1000);
fprintf('The rated current for this machine is %.2f A\n', abs(iInput)
    ↪ );
fprintf('The rated torque for this machine is %.2f N.m\n', Torque);
fprintf('The rated efficiency of this machine is %.2f%%\n', Effic
    ↪ *100);

```


Appendix B

Material Properties

The material properties were used to calculate the thermal resistances. It's based on the same material properties used in [12], and it's based on Swedish standards and international handbooks.

Material	Used in	Heat Capacitivity [J/Kg*K]	Density [kg/m ³]	Heat Conductivity [W/m.K]
Cu 99.90	Stator Winding	385	8900	395
Al 99.5	Rotor Cage	900	2705	234
Al - Si 12	Frame	960	2650	150
Steel SS1550	Shaft	460	7800	51
Unsaturated polyester	Stator Winding Impregnation	1700	1350	0.2
SURA DK-70 (1% Si)	Stator and Rotor Core	460	7800	38
air	air gap internal air ambient air	1010	1.23 at 0°C temperature coefficient -0.00278 K-1	0.0243 at 0°C temperature coefficient 69.4*10-6 K-1

Table B.1: Material Thermal Data [12]

Bibliography

- [1] B. Asad, T. Vaimann, A. Rassõlkin, and A. Belahcen. Dynamic state space model based analysis of a three-phase induction motor using nonlinear magnetization inductance. In *2018 19th International Scientific Conference on Electric Power Engineering (EPE)*, pages 1–6, 2018.
- [2] Blaz Benedik, Joze Duhovnik, Janez Rihtarsivc, and Joze Tavcar. Thermal model of through flow universal motor by means of lumped parameter network. 2017.
- [3] A. Boglietti, A. Cavagnino, and D. Staton. Determination of critical parameters in electrical machine thermal models. *IEEE Transactions on Industry Applications*, 44(4):1150–1159, 2008.
- [4] Roye D. Zhu D.S. Champenois, G. *Electrical and thermal performance predictions in inverter fed squirrel-cage induction motor drives*. *Electric Machines and Power Systems* 22 (1994) 3, p. 355-370.
- [5] A. Derdiyok, M. K. Guven, H. Rehman, and Longya Xu. A new approach to induction machine flux and speed observer with on-line rotor time constant estimation. In *IEMDC 2001. IEEE International Electric Machines and Drives Conference (Cat. No.01EX485)*, pages 102–107, 2001.
- [6] T. Du, P. Vas, and F. Stronach. Design and application of extended observers for joint state and parameter estimation in high-performance ac drives. *IEE Proceedings - Electric Power Applications*, 142(2):71–78, 1995.
- [7] M. Fan, J. Chai, and X. Sun. Induction motor parameter identification based on t-model equivalent circuit. In *2014 17th International Conference on Electrical Machines and Systems (ICEMS)*, pages 2535–2539, 2014.
- [8] Ewald F.Fuchs and Mohammad A. S. Masoum. *Power Conversion of Renewable Energy Systems*. Springer US, 2011.
- [9] A. Fitzgerald, A.E. Fitzgerald, C. Kingsley, and S. Umans. *Electric Machinery*. Electrical Engineering Series. McGraw-Hill Companies, Incorporated, 2003.
- [10] P. L. Jansen and R. D. Lorenz. A physically insightful approach to the design and accuracy assessment of flux observers for field oriented induction machine drives. *IEEE Transactions on Industry Applications*, 30(1):101–110, 1994.

- [11] G. Khoury, R. Ghosn, F. Khatounian, M. Fadel, and M. Tientcheu. Including core losses in induction motors dynamic model. In *2016 3rd International Conference on Renewable Energies for Developing Countries (REDEC)*, pages 1–6, 2016.
- [12] Gunnar Kylander. *Thermal modelling of small cage induction motors*. PhD thesis, Chalmers University of Technology, Göteborg, Sweden, 1995.
- [13] E. Levi. Iron core loss effects in indirect rotor flux oriented induction machines. In *Proceedings of MELECON '94. Mediterranean Electrotechnical Conference*, pages 766–769 vol.2, 1994.
- [14] H. Li, Q. Wang, F. Xie, C. Hu, and X. Guo. Parameters estimation of im with the extended kalman filter and least-squares. In *2015 IEEE 10th Conference on Industrial Electronics and Applications (ICIEA)*, pages 1625–1628, 2015.
- [15] Li-Cheng Zai, C. L. DeMarco, and T. A. Lipo. An extended kalman filter approach to rotor time constant measurement in pwm induction motor drives. *IEEE Transactions on Industry Applications*, 28(1):96–104, 1992.
- [16] W.V. Lyon. *Transient Analysis of Alternating-current Machinery: An Application of the Method of Symmetrical Components*. Technology Press books. Technology Press of Massachusetts Institute of Technology, 1954.
- [17] A. Marfoli, L. Papini, P. Bolognesi, D. Genovese, and C. Gerada. Analysis of induction machine: Comparison of modelling techniques. In *2017 IEEE International Electric Machines and Drives Conference (IEMDC)*, pages 1–7, 2017.
- [18] T. Matsuo and T. A. Lipo. A rotor parameter identification scheme for vector-controlled induction motor drives. *IEEE Transactions on Industry Applications*, IA-21(3):624–632, 1985.
- [19] L. Mine, S. Goyal, and A. A. E. Abdallah. Improved dynamic modeling of squirrel-cage induction machines using magnetic reluctance network theory. In *2018 21st International Conference on Electrical Machines and Systems (ICEMS)*, pages 555–559, 2018.
- [20] Tommaso Moretto. Simulation models and experimental verification of losses in induction motor drives. Master's thesis, University of Padova, Italy, 2019.
- [21] D.W. Novotny and T.A. Lipo. *Vector Control and Dynamics of AC Drives*. Monographs in electrical and electronic engineering. Clarendon Press, 1996.
- [22] D.R. Turner P.H. Mellor, D. Roberts. Lumped parameter thermal model for electrical machines of tefc design. *IEE Proceedings-B*, 138 (1991) 5, p. 205-218.
- [23] H. Toliyat, M. S. Arefeen, K. M. Rahman, and M. Ehsani. Rotor time constant updating scheme for a rotor flux oriented induction motor drive. In *Proceedings of PESC '95 - Power Electronics Specialist Conference*, volume 2, pages 1302–1306 vol.2, 1995.

- [24] H. A. Toliyat and A. A. G. Hosseiny. Parameter estimation algorithm using spectral analysis for vector controlled induction motor drives. In *ISIE '93 - Budapest: IEEE International Symposium on Industrial Electronics Conference Proceedings*, pages 90–95, 1993.
- [25] H. A. Toliyat, E. Levi, and M. Raina. A review of rfo induction motor parameter estimation techniques. *IEEE Transactions on Energy Conversion*, 18(2):271–283, 2003.
- [26] M. N. Uddin and S. W. Nam. New online loss-minimization-based control of an induction motor drive. *IEEE Transactions on Power Electronics*, 23(2):926–933, 2008.
- [27] S. Yang, D. Ding, X. Li, Z. Xie, X. Zhang, and L. Chang. A novel online parameter estimation method for indirect field oriented induction motor drives. *IEEE Transactions on Energy Conversion*, 32(4):1562–1573, 2017.